Doctoral Dissertation

Influence of laminated random heterogeneity on surface wave dispersion and radial anisotropy

（ラミナ状ランダム不均質性による表面波分散性及び
鉛直異方性への影響）

Yunao Xu

A thesis submitted for
the degree of Doctor of Philosophy

Department of Natural History Sciences
Graduate School of Science
Hokkaido University

June 2023

Abstract

A series of numerical experiments are performed to evaluate the influence of laminated stochastic heterogeneity on seismic surface waves and its potential contribution to radial anisotropy. The information derived from such numerical experiments can be the basis for interpreting real observations on large-scale seismic anisotropy in the upper mantle that are generally derived from surface wave tomography. Since the effects of such fine layering or laminated heterogeneities on surface wave dispersion have rarely been considered in tomographic studies when interpreting observed radial anisotropy, our results can provide insight into the possible cause of apparent radial anisotropy.

Recent studies on the high-frequency scattering of body waves have suggested the existence of fine-scale elongated random heterogeneity in the upper mantle. Such finely-layered heterogeneity can cause "apparent" radial anisotropy (differences in the shear wave speeds between the horizontally-polarized SH and vertically-polarized SV waves) when observed by seismic surface waves with much longer wavelength than the characteristic scale of such heterogeneity. In this study, we performed numerical experiments using 1-D and 2-D Earth models to investigate the influence of such layered or laminated velocity fluctuations on generating "apparent" radial anisotropy.

We first consider the 1-D cases, including the perturbed shear velocities relative to an isotropic reference 1-D model. Using the normal mode method, we compute the synthetic dispersion curves for the fluctuated isotropic velocity profiles. The results suggest that such layered structures would make

the effective shear modulus for SV waves smaller and that for SH waves almost unchanged from the average (or reference) model, resulting in slower Rayleigh-wave phase speeds and almost unchanged Love-wave phase speeds from the reference model, which leads to weak apparent radial anisotropy. These results are mostly consistent with the theoretical estimations based on the Backus average, which represents the long-wavelength equivalent of a layered model. However, the discrepancy between the dispersion curves from the normal-mode estimation and the Backus average becomes large for strongly heterogeneous media with large velocity fluctuations.

We also perform 2-D simulations for various laminated stochastic heterogeneities using the finite difference method (FDM). The model space extends 2000 km horizontally and 360 km vertically with 0.05 km grid spacing to incorporate the fine-scale stochastic heterogeneity. We suppose 101 virtual seismic stations located in the epicentral distances from 900 to 1900 km at a 10 km interval. 2-D simulations are performed independently for P-SV and SH waves using the same heterogeneous models. The computed seismograms in 2-D models are then used to measure single-station phase speeds of surface waves.

To extract the surface-wave phase speeds, we employ the single-station waveform fitting method for source-receiver paths based on a fully nonlinear waveform fitting with global optimization. Despite the limitations in 2-D FDM simulations, we could extract reliable average phase speed perturbations in heterogeneous models relative to the homogeneous one for both the fundamental-mode Rayleigh and Love waves in a period range from 30 to 100 s.

We investigate the influence of three main factors that control or affect the character of stochastic heterogeneity in the upper mantle based on the von Karman type distribution function; the strength of heterogeneity (the stan-

dard deviation of velocity fluctuation, σ), the lateral scale of heterogeneity (the horizontal correlation length, a_x), and the thickness of the heterogeneous layer. To consider finely laminated heterogeneity in this study, the vertical correlation length, a_z, is fixed at 0.5 km. We also consider the effective strength of velocity fluctuations, σ_{eff}, to quantify the realistic strength of heterogeneity in each 2-D heterogeneous model.

The results indicate that the strength of heterogeneity σ (or σ_{eff}) exhibits noticeable influence on the perturbation of the fundamental-mode Rayleigh wave phase speed; for models with random heterogeneity ($a_x = 5$ km and $a_z = 0.5$ km) in the depth range from 35 to 120 km, the Rayleigh-wave phase speed drop reaches around 2.0 % for $\sigma = 0.1$ ($\sigma_{eff} = 0.13$), and around 0.5 % for $\sigma = 0.05$ ($\sigma_{eff} = 0.066$), depending on periods. For weaker heterogeneity, the influence on phase speed can be almost negligible. The changes in the horizontal correlation length a_x also show some influence; for larger a_x, phase speed reduction becomes greater, although we could confirm it only for limited cases. The results of the varying thicknesses of the heterogeneous layer suggest that their influence on phase speed perturbations mostly reflects the vertical sensitivity of Rayleigh waves as a function of periods. In all cases, the influence on the fundamental-mode Love waves is insignificant. Through these numerical experiments, we could confirm how laminated stochastic heterogeneity affects surface-wave dispersion.

We then invert for 1-D radially anisotropic S wave models using the phase speed perturbations of the fundamental-mode Rayleigh and Love waves for specific stochastic models. The results indicate that, for $\sigma_{eff} = 0.1$, the expected apparent radial anisotropy can be about $\xi \approx 1.04$, which can be nearly half of the observed radial anisotropy commonly seen in tomographic models. For a case with $\sigma_{eff} = 0.05$, apparent radial anisotropy can be about $\xi \approx 1.01$. The results obtained in this study suggest that the laminated

heterogeneity with specific properties may generate a certain level of apparent radial anisotropy, and the observed radial anisotropy could be partially attributed to the existence of laminated random heterogeneity.

Acknowledgements

I would like to give my heartfelt thanks to all the people who ever helped me finish this thesis and through my study at Hokkaido University.

My sincere thanks and appreciations go firstly to my supervisor, Professor Kazunori Yoshizawa, without whom this work could have never been done. It has been a great privilege and honor to study under his supervision for the past 8 years. It is always something to be enjoyed when having a conversation with him. His guidance and knowledge never failed to help me when I had problems in my study and life. It is my honor to benefit from his personality and diligence, which I will treasure for my whole life. Thank you, professor, my gratitude for you know no bounds.

I am also extremely grateful to Professor Kiyoshi Yomogida for all the essential and sharp comments he gave me about this study and many others. It was not easy to answer his questions because he could easily find the key problem of my presentation, and I really benefited a lot from that.

Professor Takashi Furumura has kindly shared his code for generating heterogeneous models and given me many instructions on how to use it correctly. He has been the co-author for many of my presentations, and he was always eager to help.

I also thank Kouta Hamada, Hitoshi Matsuzawa, Ryo Narita, Toru Taira, and all the current and past members of the Seismology Lab and Solid Earth Seminar, for some have kindly given advice on my research, and others brought me to help on the study and my life in Japan. I am also grate-

ful for many researchers who gave advice on meetings and workshops.

Finally, my heartful thanks go to my family and friends who love and care for me and whom I love and care for. I am especially thankful to my wife, who gave unconditional love and support to my study and life.

During my PhD course, The Chinese Scholarship Council supported my life in Japan and covered my traveling expenses. I used MINEOS v1.0.2 for normal mode calculation and GMT 6 for making figures. Most of my 2-D modeling uses the EIC system of the Earthquake Research Institute, University of Tokyo.

Contents

Chapter 1

Introduction

Seismic anisotropy, which reflects the directional dependence of seismic wave speeds, has been one of the major targets of extensive research in seismology. It provides us with invaluable information on the internal structure and dynamic processes of the Earth. Seismic surface waves (Love and Rayleigh waves), which are sensitive to both heterogeneity and anisotropy, especially in the crust and upper mantle, can be powerful tools in studying them. In this chapter, we first briefly review the background of surface wave propagation, seismic anisotropy, and heterogeneity. Then, we will overview the contents and scope of this study.

1.1 Surface waves in heterogeneous and anisotropic media

Seismic surface waves (Love and Rayleigh waves) have been used as an effective tool for investigating the large-scale spatial variations of both heterogeneity and anisotropy in the upper mantle. Surface waves are sensitive to the shallow layers of the Earth, such as the crust and upper mantle, and the arrival time anomalies of surface waves reflect the lateral heterogeneity of velocity structure in general, which can be used to build surface-wave dispersion maps (e.g., Ekström et al., 1997; Ekström, 2011). The dispersive

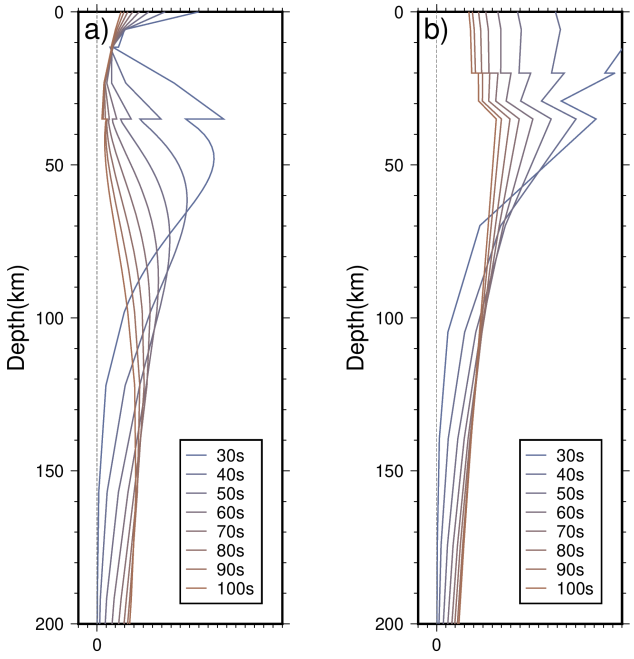

Figure 1.1: Sensitivity kernels of the fundamental-mode phase speed to the S-wave speed in a period range of 30 – 100 s. (a) Rayleigh wave, and (b) Love wave.

character of surface waves enables us to investigate the vertical variation of seismic velocity structure since surface waves at different periods are sensitive to different depth ranges (e.g., Takeuchi & Saito, 1972). Fig. 1.1 shows some examples of the vertical sensitivity kernels of the fundamental-mode Rayleigh and Love waves to shear velocities in the period range from 30 to 100 s.

Surface waves have also been extensively used to retrieve the 3-D distribution of radial and azimuthal anisotropy in the upper mantle. Azimuthal anisotropy can be detected from the difference in phase speeds at different propagation directions using surface waves. Radial anisotropy (or transverse isotropy with a vertical symmetry axis; TIV or VTI) reflects wave speed differences between horizontally-polarized SH waves (V_{sh}) and vertically-polarized SV waves (V_{sv}), which is defined as $\xi = (V_{sh}/V_{sv})^2$. Observations

of both Rayleigh (sensitive to SV) and Love (sensitive to SH) waves allow us to map the 3-D variations of azimuthal and radial anisotropy in the Earth.

However, the resolution of surface wave studies is generally limited due to the long-wavelength nature of surface waves. Seismic waves are essentially insensitive to the details of smaller-scale structures than the wavelength, and their propagation may depend on the spatial average structure (e.g., Capdeville et al., 2013; Fichtner et al., 2013; Jordan, 2015). Many studies have been done on small-scale heterogeneities in the Earth, which will be further discussed in the subsequent section 1.3, but most of them have focused primarily on body waves at higher frequencies rather than surface waves at lower frequencies.

Tomographic studies using surface waves generally aim to retrieve large-scale deterministic heterogeneity in the mantle, and the smaller-scale structure relative to their wavelength is generally not considered (Fichtner et al., 2013; Capdeville et al., 2013). Therefore, the effect of such small-scale heterogeneity on long-period surface waves and radial anisotropy has not been studied well compared to the extensive research on body wave scattering.

1.2 Observations of seismic anisotropy in the upper mantle

Recent seismic studies using long-period surface waves have revealed large-scale radial anisotropy with $V_{sh}>V_{sv}$ in the lithosphere and asthenosphere both in oceanic and continental regions (e.g., Nettles & Dziewoński, 2008; Yuan & Romanowicz, 2010; Yoshizawa, 2014; Isse et al., 2019). Yuan & Romanowicz (2010) revealed the two-layer structure of North American craton, with vertical variations in azimuthal anisotropy. Nettles & Dziewoński (2008) found strong lateral variations of radial anisotropy; e.g., continental plates tend to have a thick and strongly anisotropic layer, and significant

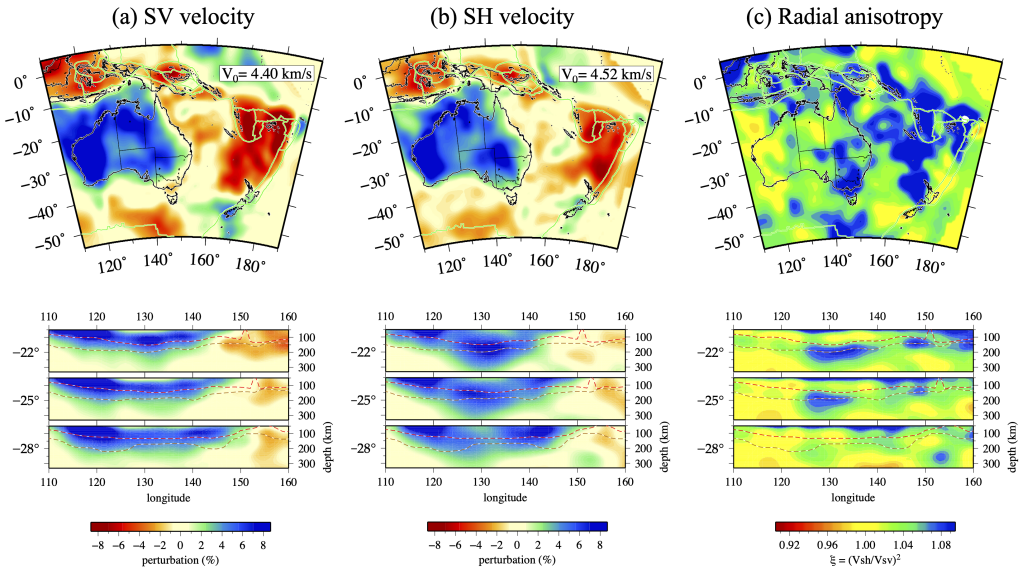

Figure 1.2: Radially anisotropic S-wave tomography model in Australia by Yoshizawa (2014). (a) SV wave velocity, (b) SH wave velocity, and (c) Radial Anisotropy $\xi = (V_{sh}/V_{sv})^2$. (Top) map projections at 75 km depth, (bottom) east-west cross sections at 22°S, 25°S, and 28°S.

radial anisotropy with $V_{sh} > V_{sv}$ beneath the Pacific plate, which has also been confirmed by recent studies using ocean-bottom seismometers in the Pacific (Isse et al., 2019).

Observed radial anisotropy can be explained by a combination of the effects from both the lattice-preferred orientation (LPO) and shape-preferred orientation (SPO) (Magali et al., 2021), since it can arise either from intrinsically anisotropic media or isotropic layering. Thus, the lateral and vertical variations in radial anisotropy may be partially attributed to the structural variations in the Earth.

Recent studies in Australia using multi-mode surface wave tomography (Fig. 1.2) have found that the strength of radial anisotropy drops rapidly within the continental lithosphere near the depths of Mid-Lithosphere Discontinuity (MLD), while the shallow lithosphere and asthenosphere tend to

show very strong radial anisotropy with $V_{sh} > V_{sv}$ (e.g., Yoshizawa, 2014; Yoshizawa & Kennett, 2015). The heterogeneity in the mantle has strong spatial variations for both SV and SH wave speed structures, which leads to changes in radial anisotropy at a certain depth in the lithosphere. Such a rapid vertical change within the lithosphere can be related to the enigmatic MLD (Kennett & Furumura, 2016; Sun et al., 2018), often observed in the cratonic lithosphere from the receiver functions (Ford et al., 2010; Birkey et al., 2021; Taira & Yoshizawa, 2020).

1.3 Stochastic heterogeneity in the lithosphere

The Earth is heterogeneous at a variety of scales, and its physical properties vary at different locations. The difference between heterogeneity and anisotropy is more of a problem in scale since every heterogeneous material can also be, at some scale, anisotropic (Bodin et al., 2015; Maupin & Park, 2015).

Various geophysical observations, including high-frequency scattering and P wave reflectivity, have suggested the existence of fine-scale quasi-laminar structures in the continental and oceanic lithosphere. Nielsen et al. (2003) suggested an inhomogeneous zone in the upper mantle that can be described by random velocity fluctuations to explain the high-frequency signals that propagate long distances (>2000 km) from PNE (peaceful nuclear explosion) data in Russia. Furumura & Kennett (2005) and Kennett & Furumura (2008) performed numerical simulations of seismic wavefields to explain the extended coda after both P and S wave arrivals from a deep earthquake in the subduction zone. They have suggested that such coda waves can be generated by the waveguide effect from quasi-laminated heterogeneity in the subducting plate. Their results from the numerical simulations well represented actual observations.

Kennett et al. (2013) and Kennett & Furumura (2016) extended their target to oceanic cases in the northeast Pacific and continental paths inside Australia, respectively. These studies used stochastic heterogeneity with a horizontal correlation length of 10–20 km in the lithospheric mantle and a shorter horizontal correlation length for the crust of about 5 km. On the other hand, P wave reflectivity studies in Australia using auto-correlograms at seismic stations have also indicated the presence of strong heterogeneity throughout the lithosphere and even in the upper asthenosphere, with a scale length of 300–500 m in the uppermost mantle (Kennett, 2015). Their study also found no clear tie for the patterns of reflectivity between closely spaced stations (about 50 km interval), which is consistent with the horizontal correlation length suggested by high-frequency observations.

While only relatively mild heterogeneity (about 1 % fluctuation) is required down to 100 km for generating the long P and S wave coda, P wave reflectivity in some areas has suggested the existence of strong heterogeneity near the lithosphere-asthenosphere transition (LAT) (Sun & Kennett, 2017; Kennett et al., 2017).

The existence of such laminated heterogeneity would result in apparent (or effective) radial anisotropy on a larger scale. Thus, it will be essential to quantify the effect of such laminated heterogeneity on observed large-scale anisotropy, primarily constrained by longer-period surface waves (e.g., Nishimura & Forsyth, 1989; Gung et al., 2003; Nettles & Dziewoński, 2008; Yoshizawa, 2014).

1.4 Structure induced seismic anisotropy

Seismic anisotropy can be linked to the lattice-preferred orientations (LPO) of intrinsically anisotropic crystals, providing valuable information about geodynamic processes in the Earth. However, the effects of LPO are not the only

cause of seismic anisotropy. It has been recognized that radial anisotropy can also arise from structural characteristics of isotropic media, e.g., fine layering (Aki, 1968; Allegre & Turcotte, 1986), aligned cracks with fluid inclusion (Thomsen, 1995; Hudson et al., 2001), or partial melting (Kawakatsu et al., 2009; Hirschmann, 2010). This type of elastic anisotropy caused by inhomogeneities on a relatively small scale compared to the wavelength of seismic waves is sometimes called the shape-preferred orientation (SPO), in contrast to the LPO.

In the ideal case of SPO, a purely isotropic layered medium is equivalent to a vertical transversely isotropic (VTI) medium in the long period, when the wavelength employed is much longer than the average thickness of each layer (Backus, 1962). The Backus theory, or the Backus average, tells us that fine layering of isotropic materials can cause changes in the effective shear modulus of the layered medium. The effective shear modulus is a measure of the overall rigidity of the medium, as described using laminated alternating layers of hard and soft materials Aki (1968).

Studies on this type of anisotropy used different epithets to describe it, for example, shape-preferred orientation (SPO), apparent anisotropy (Fichtner et al., 2013), extrinsic anisotropy (Wang et al., 2013; Faccenda et al., 2019), geometric anisotropy (Jordan, 2015), and effective anisotropy (Maupin & Park, 2015). In this paper, we use "apparent anisotropy" to describe the large-scale anisotropy that arises from the layered isotropic media or laminated fine-scale heterogeneities that comprise isotropic materials. Some earlier studies, such as Fichtner et al. (2013) and Wang et al. (2013), discussed the influence of intrinsic anisotropy from LPO and apparent (extrinsic) anisotropy from isotropic layering. Fichtner et al. (2013) concluded that the observed seismic anisotropy could be explained by purely isotropic layering unless all anisotropic parameters are known well. Meanwhile, Wang et al.

(2013) suggested that observed radial anisotropy can be a linear combination of LPO-induced intrinsic anisotropy and apparent (extrinsic) anisotropy related to fine layering. They concluded that fine layering could be an important contributor to explaining the observed seismic anisotropy in the upper mantle. Thus, the observed radial anisotropy would be very unlikely to be entirely intrinsic or apparent, but observed anisotropy is likely to be, in general, a combination of the two causes.

It should be noted that most of the studies mentioned above considered the body wave case. To our best knowledge, the discussion of such heterogeneity on surface wave dispersion has been considered only by a few authors like Capdeville & Marigo (2007) and Dalton et al. (2019). Their earlier studies are of great importance in understanding this problem, but generally, they considered simplified cases with isotropic alternating layers or stratified models with inhomogeneities.

Therefore, more extensive studies are required to clarify the relationship between layered random heterogeneity of isotropic materials inferred from high-frequency body wave studies and observed radial anisotropy derived from long-period surface wave studies.

1.5 The scope of this study

The aim of this study is to investigate the relationship between the laminated random heterogeneity in 1-D and 2-D media and radial anisotropy observed from seismic surface waves, through extensive numerical experiments of normal-mode calculations and seismic wavefields of broad-band seismic waves from the finite-difference method.

In chapter 2, we briefly review the effective medium theory originally developed by Backus (1962). By employing numerical experiments based on normal mode calculations with isotropic 1-D layered models with velocity

fluctuations in the uppermost mantle, we investigate how such layered media would affect the surface wave phase speeds, compared with the theoretical estimation from the Backus average for long-period surface waves. We confirm that such layered structures would make effective shear modulus for vertically polarized SV waves smaller, while that for horizontally polarized SH waves can be almost unchanged from the average (or reference) model. This leads to the "apparent radial anisotropy", and results in slower Rayleigh wave phase speeds, while the Love wave phase speeds are nearly unchanged from the reference model.

In chapter 3, we perform a variety of 2-D forward modeling with the finite-difference method (Furumura & Kennett, 2005; Kennett & Furumura, 2008) to compute the seismic wavefields in homogeneous and heterogeneous media, including various strengths and scales of stochastic heterogeneities. We employ a single-station waveform fitting method (Yoshizawa & Ekström, 2010) to measure the phase speeds of surface waves propagating in these different 2-D models. The careful investigations of extracted dispersion curves allow us to confirm their reliability. By taking the ensemble average of measured phase speeds from finely laminated heterogeneous models, we can estimate the average phase speed perturbations of the fundamental-mode Rayleigh and Love waves relative to the homogeneous reference model, which represents the effect of laminated stochastic heterogeneity on long-period surface waves. We discuss the effect of a variety of stochastic heterogeneities, particularly on Rayleigh wave phase speeds.

In chapter 4, based on the results derived from chapters 2 and 3, we discuss the plausible radial anisotropy that can be caused by laminated stochastic heterogeneities, and how it could be related to actual observations. For the quantitative interpretation of the apparent radial anisotropy, we perform inversions of surface-wave phase speeds derived in the earlier chapter for the

vertical 1-D profiles of radially anisotropic S-wave models. Based on the retrieved anisotropic parameter ξ, we quantitatively evaluate the plausible influence of laminated heterogeneity on apparent radial anisotropy.

In chapter 5, we summarize the work done in this thesis and discuss some additional topics to be investigated in the future.

Chapter 2

Layered structure and radial anisotropy: normal-mode approach with 1-D model

As discussed in the introduction, observed radial anisotropy in the Earth is generally a combination of different causes of seismic anisotropy. In this study, we mainly focus on radial anisotropy that can also be generated from finely layered or quasi-laminated structures.

In this chapter, we will first review anisotropic properties in layered media following earlier studies of seismic wave propagation and how fine-scale horizontal layering could induce apparent radial anisotropy. Then, a series of numerical experiments using 1-D velocity models are performed to check the effect of such layered structures on long-period surface wave phase dispersion.

2.1 Structure-induced radial anisotropy by horizontal layering

The study of seismic wave propagation in layered media has a long history of over a century (e.g., Voigt, 1928; Reuss, 1929; Backus, 1962; Aki, 1968). To simplify the complexity of the problem, we start with an elastic medium with transversely isotropic layers with a vertical symmetry axis (VTI medium). Each layer can be described using density ρ and five elastic parameters a, c, f, l and n (Love, 1927).

Following the discussion given by Backus (1962), when the wavelength employed is much longer than a certain distance over the heterogeneous layer, wave propagation through a finely layered VTI medium can be described by its long wavelength equivalent. The effective elastic parameters can thus be calculated using upscaling functions (e.g., Bodin et al., 2015):

$$\begin{aligned} A &= \langle a - f^2 c^{-1} \rangle + \langle c^{-1} \rangle^{-1} \langle f c^{-1} \rangle^2, \\ C &= \langle c^{-1} \rangle^{-1}, \\ F &= \langle c^{-1} \rangle^{-1} \langle f c^{-1} \rangle, \\ L &= \langle l^{-1} \rangle^{-1}, \\ N &= \langle n \rangle, \end{aligned} \tag{2.1}$$

where the bracket $\langle\rangle$ represents the spatial average over a certain distance of any given function. Supposing that each layer inside this medium is isotropic (i.e., $a = c = \lambda + 2\mu$, $f = \lambda$, $l = n = \mu$), the effective elastic parameters can be given by:

$$\begin{aligned} A &= \langle 4\mu(\lambda + \mu)(\lambda + 2\mu)^{-1} \rangle + \langle (\lambda + 2\mu)^{-1} \rangle^{-1} \langle (\lambda + 2\mu)^{-1} \rangle^2, \\ C &= \langle (\lambda + 2\mu)^{-1} \rangle^{-1}, \\ F &= \langle (\lambda + 2\mu)^{-1} \rangle^{-1} \langle \lambda(\lambda + 2\mu)^{-1} \rangle, \\ L &= \langle \mu^{-1} \rangle^{-1}, \\ N &= \langle \mu \rangle. \end{aligned} \tag{2.2}$$

Note that N and L that are equivalent to the shear modulus for SH and SV wave speeds can be given by the arithmetic mean and harmonic mean of shear modulus μ, respectively. Unless μ remains constant among all layers, $N > L$. This indicates that the layered medium is effectively anisotropic on a long wavelength. The radial anisotropy parameter ξ can be represented as,

$$\xi = N/L = \langle \mu \rangle / \langle \mu^{-1} \rangle^{-1}. \tag{2.3}$$

Thus, a 1-D model with fine-scale isotropic layers with fluctuated elastic properties would generally show radial anisotropy as $V_{SH} > V_{SV}$ when observed by long-wavelength seismic waves. This phenomenon is the well-known radial anisotropy induced by horizontal layering (e.g., Backus, 1962; Aki, 1968).

With the analytical expressions for the effective elastic parameters in a 1-D stratified medium by Backus (1962), we can directly calculate the level of radial anisotropy that can be caused by a 1-D structure with thin layers. Consider a 1-D stratified model which has m isotropic layers. For i-th layer, the thickness is h_i and the shear modulus is μ_i. Then, the effective elastic parameter N and L can be represented as follows,

$$N = \frac{1}{H}\sum_{i=1}^{m}\mu_i h_i, \tag{2.4}$$

$$L = H/\sum_{i=1}^{m}\frac{h_i}{\mu_i}, \tag{2.5}$$

$$H = \sum_{i=1}^{m} h_i, \tag{2.6}$$

where H represents the total thickness.

Supposing that each layer has the same thickness, the above function can be simplified as,

$$N = \frac{1}{m}\sum_{i=1}^{m}\mu_i, \tag{2.7}$$

$$L = m/\sum_{i=1}^{m}\frac{1}{\mu_i}. \tag{2.8}$$

Note that μ is the shear modulus for isotropic media ($\mu = \rho\beta^2$), where β is shear velocity and ρ density. For any given 1-D isotropic model with fine layers, we can numerically calculate its long wavelength equivalent, which will be considered in the next section.

It should be noted that the Backus theory assumes seismic waves propagating across the heterogeneous layer with fine layering, like near-vertically

propagating body waves. Therefore, it may not necessarily work properly for describing surface wave dispersion which propagates horizontally. Dalton et al. (2019) have recently studied the limitations of the Backus average on guided waves (or surface waves). While their studies mainly focused on higher frequency ranges used in exploration seismology, their results showed that the Backus average is insufficient to describe the surface wave dispersion in strongly heterogeneous non-alternating layers, and it works for limited cases with weak inhomogeneity and lower frequency. Capdeville & Marigo (2007) considered effective medium theory to avoid the high computational cost of numerical approach with fine grids, and their result showed that, while the Backus theory gives good estimation for body wave velocity, it cannot provide a correct result for surface wave phase speeds. Therefore, there is an intrinsic limitation of the Backus average when we study the effect of fine-scale heterogeneity on surface wave propagation. Thus, a numerical approach taking account of fine girds can be a more direct way to solve this issue, which is the main approach of this study.

2.2 Numerical experiments using 1-D models

In this section, we performed a series of 1-D numerical experiments to compute the phase speed anomalies of surface waves using 1-D S-velocity models with fluctuating velocities at a certain depth range. We used a program package, MINEOS v1.0.2 (Masters et al., 2011) for the normal mode calculations using 1-D Earth models.

We consider 1-D models with random fluctuations (at 35–120 km depth) from the reference Earth model iasp91 (Kennett & Engdahl, 1991). For simplicity, S-wave velocity at each depth is randomly fluctuated, while the other parameters are unchanged from the reference model. Unlike the 2-D random models discussed in the next chapter, here we do not consider any particular spectral density distribution that represents the spectral power of heterogeneity in the wavenumber domain.

The normal mode calculation has a limitation in incorporating extremely thin layers with rapid velocity changes. Thus, we fixed the thickness of each layer to 1 km, allowing enough randomness in the 1-D models while keeping the stability of normal mode calculations. The shear velocity at each layer is calculated by adding a random perturbation to the reference model. The velocity perturbation at each layer is controlled by a random distribution of Gaussian type. The average velocity perturbation is set to zero with a specific standard deviation σ (strength of heterogeneity) to simulate the finely layered model with stochastic velocity fluctuations. Fig. 2.1 shows some examples of random models generated and the corresponding dispersion curves for the fundamental-mode Rayleigh and Love waves in comparison with those for the reference model iasp91.

Figs. 2.2 and 2.3 display the resultant Rayleigh and Love wave phase speed perturbations for $\sigma = 0.05$ and $\sigma = 0.1$ cases, respectively. For each case, we generated 1000 models in total and calculated Rayleigh and Love

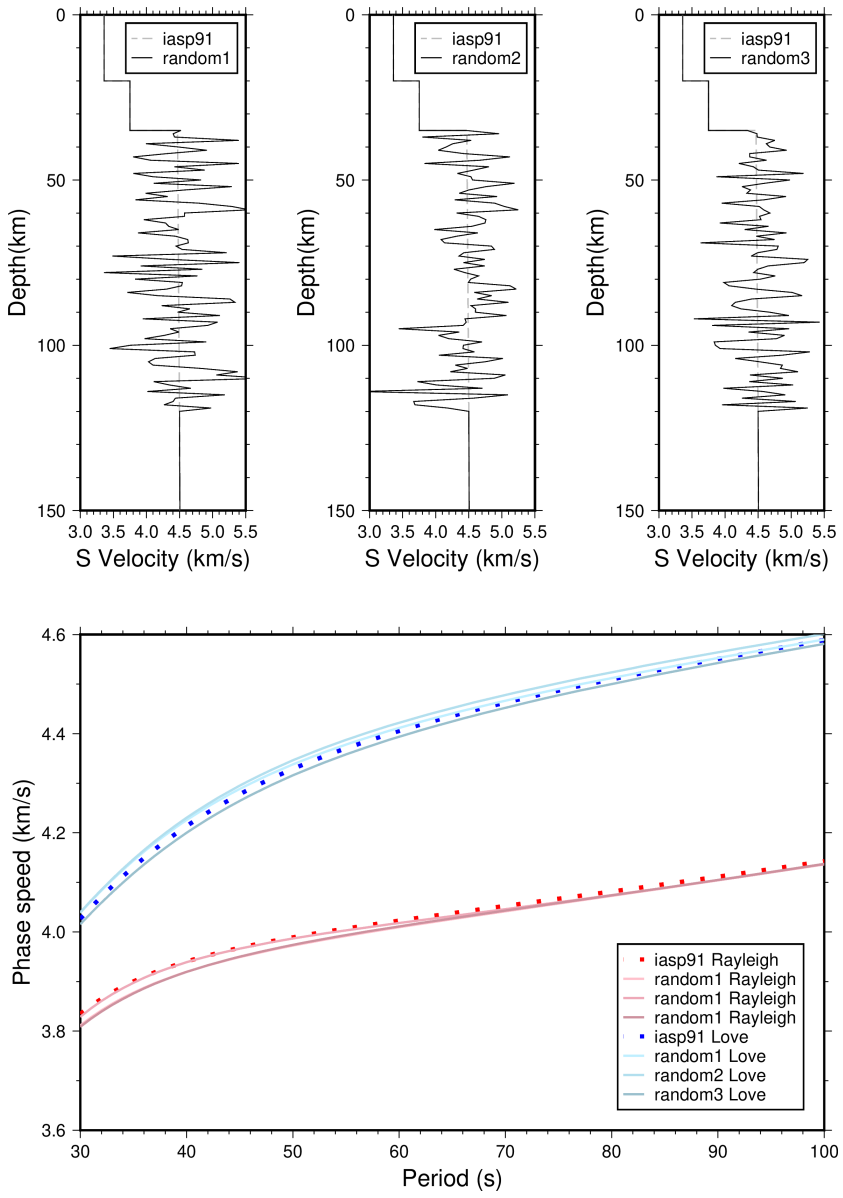

Figure 2.1: Examples of 1-D models with random velocity fluctuations from a reference model iasp91 (the standard deviation of velocity fluctuation $\sigma = 0.1$) in the depth range from 35 to 120 km. (Top) 3 selected random models, and (bottom) their corresponding dispersion curves for both Rayleigh and Love waves.

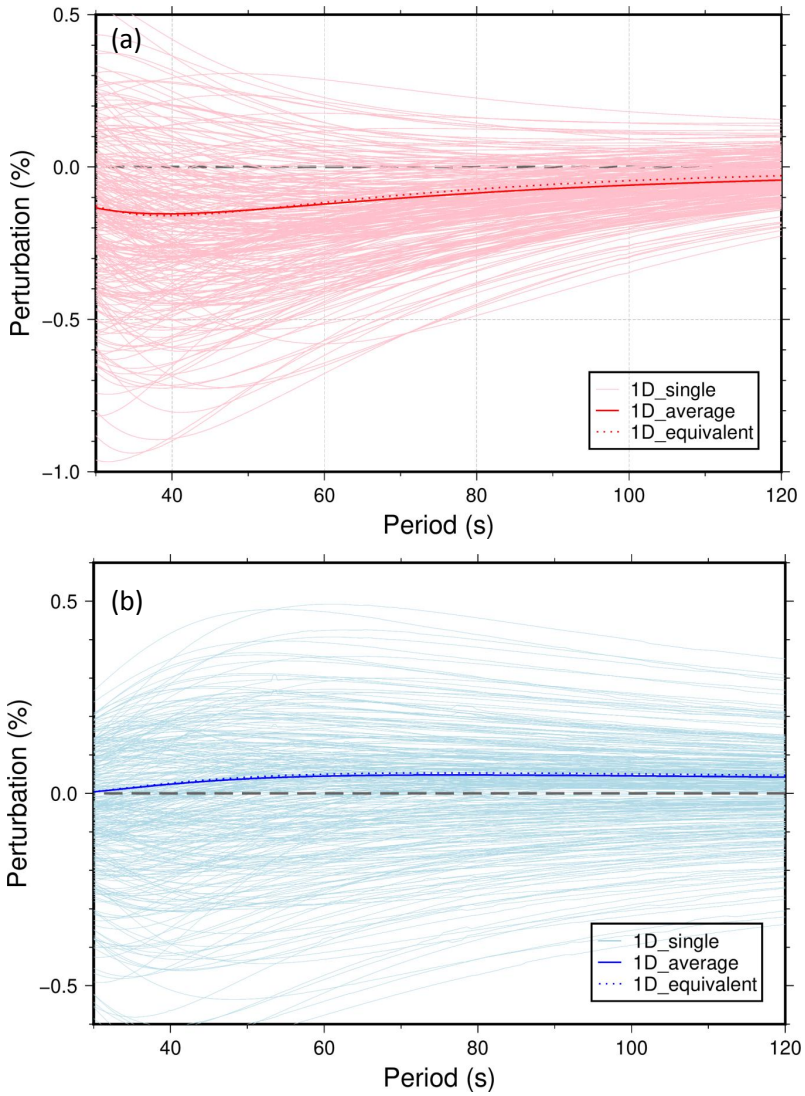

Figure 2.2: Phase speed perturbations relative to the reference model for 1000 1-D random models (thin solid line) with the standard deviation of velocity fluctuations $\sigma = 0.05$, the average phase speed perturbation from the 1000 models (thick solid line), and theoretical estimation from the Backus-average (the long wavelength equivalent) model (dotted line), for (a) Rayleigh wave (red) and (b) Love wave (blue).

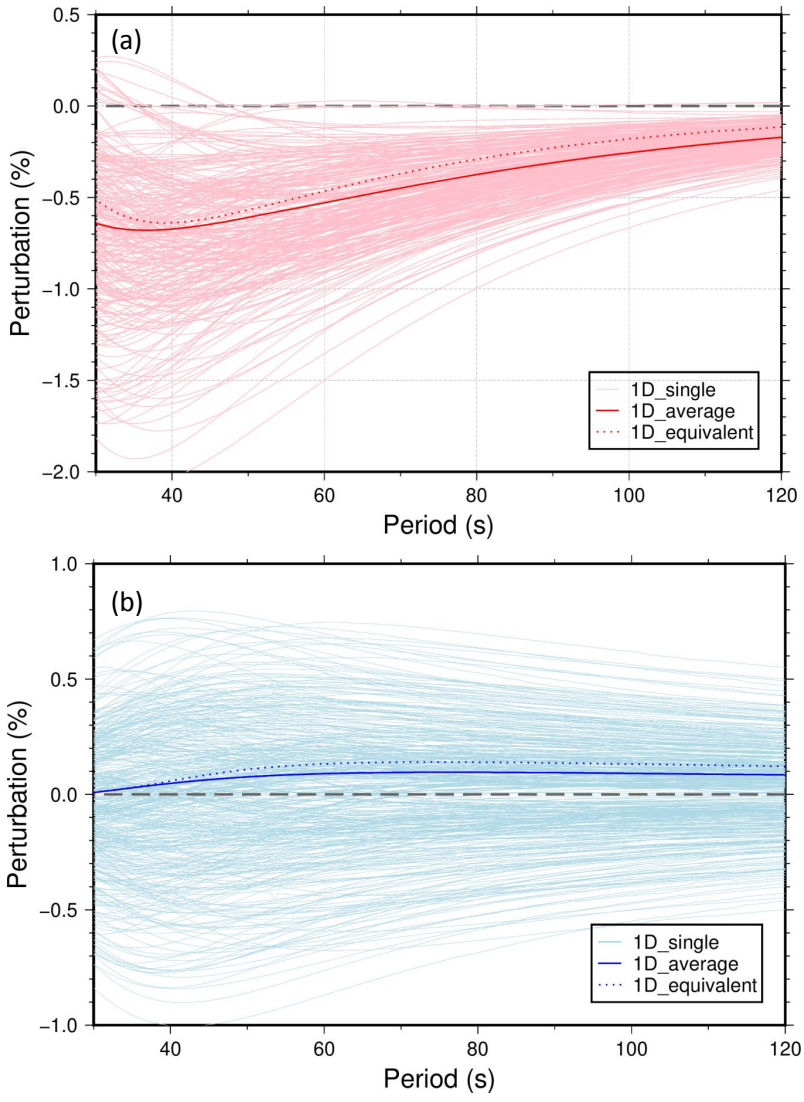

Figure 2.3: Same as Fig. 2.2, but for $\sigma = 1.0$.

wave phase speed perturbations relative to the reference model. Then, we take the average of all models so that the average influence of the stochastic model on surface wave dispersion can be extracted.

These results suggest that the surface wave phase speeds show large variations for individual random models. However, the ensemble average of phase speed perturbations from a large number of models becomes closer to the Backus average, in particular, for smaller velocity fluctuations ($\sigma = 0.5$). For larger σ ($= 1.0$), the discrepancy between the ensemble average and the Backus average becomes larger, which is consistent with earlier studies (Capdeville & Marigo, 2007; Dalton et al., 2019).

In either case, the average phase speed for the Rayleigh waves tends to be slower due to the S-wave velocity fluctuations in 1-D models. The average phase speed for the Love waves shows a slightly positive anomaly relative to the reference model due to the slight increment of effective shear modulus with fluctuated S-wave velocity (with fixed density), although the phase speed difference is much smaller than the Rayleigh wave case. These results coincide well with theoretical predictions in the previous section for layered medium, as the Rayleigh waves (sensitive to SV waves or L in (2.2)) show negative anomalies, while the Love waves (sensitive to SH waves or N in (2.2)) remain less changed.

The current numerical experiments with 1-D models with a 1-km grid suggest that the effect of fine layering on surface wave dispersion is not very significant in general; with 10 % shear velocity fluctuations, it would generate about 0.5 – 0.7 % phase speed drop on average for Rayleigh waves, and Love waves are less affected with little difference from the reference model (less than 0.1 %). These 1-D numerical experiments are simple trial tests to investigate how such layered structures would affect surface wave dispersion. We have employed simplified 1-D models with a fixed layer thickness of 1

km due to the limitations of normal mode calculation, which have difficulty in incorporating thinner layers. Also, as explained earlier, the S-wave velocity at each depth has randomly fluctuated, but the other parameters are unchanged from the reference model for simplicity. Moreover, 1-D normal mode computation does not directly reflect the process of surface wave propagation in laterally heterogeneous media, including random heterogeneity, which will be further discussed in detail in the next chapter.

Chapter 3

Influence of laminated random heterogeneity on surface wave phase speeds: 2-D FDM approach

In the previous chapter, we investigated how the 1-D layered models with rapid velocity fluctuations affect the phase speeds of surface waves. Now in this chapter, we will further investigate the influence of laminated random heterogeneity on surface wave phase speeds based on the numerical waveform simulations with the finite-difference method. The computed synthetic seismograms are then used to measure single-station phase speeds to estimate how such random heterogeneities will affect surface wave propagation, which eventually generates apparent radial anisotropy.

3.1 Numerical waveform modeling in 2-D heterogeneous media

As discussed in Chapter 1.3, fine layering or horizontally elongated heterogeneity in the Earth would cause apparent seismic anisotropy, which can be observed as anomalous phase speeds of long-period surface waves with respect to the background isotropic models. Still, it is not a straightforward issue to distinguish the cause of such anisotropy in actual seismic observations, since observed anisotropy is generally a combination of different causes;

e.g., intrinsic anisotropy due to anisotropic materials and/or flow-induced lattice-preferred orientation, and apparent anisotropy due to shape-preferred orientation and/or fine layering (e.g., Babuska & Cara, 1991; Fichtner et al., 2013). Numerical waveform modeling may provide us with a hint at the relationship between the elongated heterogeneity in an isotropic medium and apparent radial anisotropy due to the structural heterogeneities, which can be observed as phase speed anomalies of long-period surface waves.

The 1-D numerical experiments in Chapter 2.2 help to understand the fundamental aspects of the problem, but such analyses based on 1-D models alone are insufficient as heterogeneity in the real Earth varies in a 3-D space. While it would be ideal for performing full 3-D forward simulations for seismic wavefields, the high-resolution meshes ($\sim$ 0.1 km) required to study such fine-scale heterogeneity on a large-scale structure (over several thousand kilometers laterally and several hundred kilometers vertically) make such computations prohibitive even with the recent computing facilities. In particular, we need to run such simulations repeatedly with a variety of parameter settings. Therefore, to investigate the effects of fine-scale laminated heterogeneity on phase speeds of long-period surface waves, which propagate over a long epicentral distance, we performed a series of numerical simulations with the finite-difference method (FDM) with two-dimensional models by Furumura & Kennett (2005) and Kennett & Furumura (2008) incorporating multiple combinations of different model parameters.

In this section, we summarize the method of waveform modeling in 2-D media, including fine-scale laminated heterogeneity. The synthetic waveforms generated from such numerical simulations will be utilized in the next section to measure phase speeds of long-period surface waves, to quantitatively evaluate the apparent radial anisotropy caused by a variety of laminated heterogeneities.

3.1.1 Model settings for 2-D wavefield simulations with FDM

The numerical modeling technique employed in this study is based on earlier studies by Furumura & Kennett (2005) and Kennett & Furumura (2008). Here we summarize the method and models used throughout this study. We first consider a stratified model with a simulation domain of 2000 km horizontally and 360 km vertically (Fig. 3.1). P-SV and SH wavefields are simulated separately, using a uniform grid size of 0.05 km, so we have adequate spatial sampling for the fine-scale heterogeneity. The source was placed at 100 km from the left side of the model and at a shallow depth of 5 km. A total of 101 virtual stations were placed on the right half of the model with a station interval of 10 km, so the longest epicentral distance is 1900 km, and the shortest one is 900 km. We employed a conventional absorbing buffer zone (Cerjan et al., 1985) of 20 grid-points width on both sides and bottom of the model in order to minimize artificial reflections from the boundaries. The simulation is performed for each model to compute the full wavefields for P-SV and SH waves independently. This simulation takes a CPU time of approximately 24 hours by parallel computing using 160 cores of the EIC system (Earthquake Research Institute, The University of Tokyo) for P-SV waves and around 12 hours for SH waves, respectively.

The velocity model is generated by adding stochastic heterogeneities into the background model with homogeneous layers, introducing the fine-scale random heterogeneities in the upper mantle. We perturbed P-wave velocity, S-wave velocity, and density in the background model. The background model is generated from the combination of different reference models, where the V_P and V_S values are derived from the iasp91 model (Kennett & Engdahl, 1991), density ρ is taken from PREM (Preliminary Reference Earth Model) (Dziewonski & Anderson, 1981) and Q is determined following Robertsson et al. (1994). The finely laminated structure can be modeled by introducing

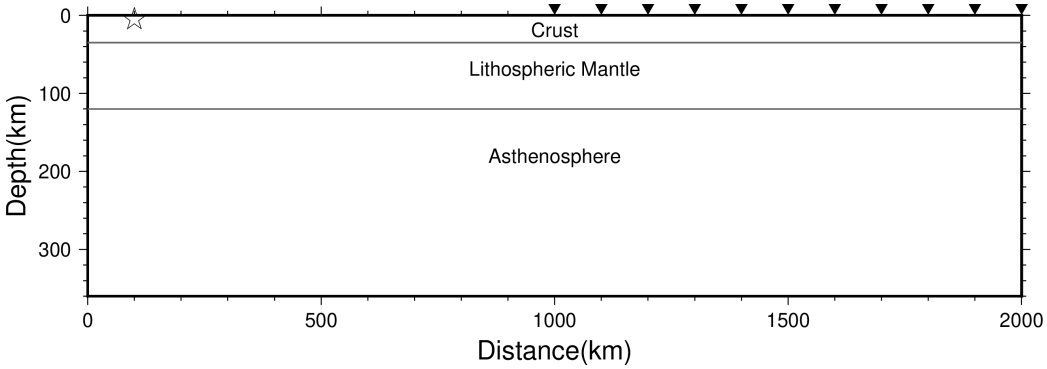

Figure 3.1: Model configuration for the flat-layered model. The seismic source is shown as a white star in the crust at 5 km depth. Selected locations of the imaginary seismic stations (from 1000 km to 2000 km, 101 stations in total) are shown in black inverse triangles.

the von Karman type stochastic heterogeneity (Frankel & Clayton, 1986) with a relatively longer horizontal correlation length, which can be added to each layer of the background model. Also, the Earth flattening correction is applied to take account of the effect of Earth's sphericity, which needs to be considered on a large scale assumed in this study. The actual structure of the Earth includes large-scale structural variations, such as the varying thickness of the lithosphere and slab subduction. However, to simplify the problem and focus on the influence of fine-scale random heterogeneity, we consider a flat layered model with random heterogeneity confined in a specific depth range.

As an initial numerical experiment for 2-D forward modeling, we start with a flat Earth model containing laminated heterogeneities with the von Karman type random deviations from the background velocity in the depth range of 35–120 km, representing horizontally elongated random heterogeneities in the mantle lithosphere. We first generated Gaussian random numbers in the spatial domain with an average value of 0, then transferred them into the wavenumber domain using the fast Fourier transform (FFT). We employed a spatial filter in the wavenumber domain using the probability

density function P based on the von Karman type distribution with a Hurst number (κ) of 0.5, vertical correlation scale a_z as 0.5 km, and varying horizontal correlation scale a_x as we will discuss later. The probability density distribution in terms of horizontal slowness p and vertical slowness q takes the form (e.g., Kennett & Furumura, 2013, 2015, 2016):

$$P(p,q) = \frac{4\pi\kappa\sigma^2 a_x a_z}{(1+\omega^2 a_x^2 p^2 + \omega^2 a_z^2 q^2)^{\kappa+1}}, \tag{3.1}$$

where σ controls the velocity fluctuation with respect to the reference (representing the strength of heterogeneity). Then, we can obtain the random heterogeneity model in the spatial domain by taking the inverse Fourier transform. Generated heterogeneities are directly used as velocity perturbation from the background model for P and S wave velocities, and multiplied by a scaling factor of 0.8 for the perturbation of density ρ.

Fig. 3.2 shows an example of a 2-D heterogeneous model and selected 1-D profiles of shear velocity at different locations. This example model incorporates horizontally elongated stochastic heterogeneity of $\sigma = 0.05$, a_x=5 km and a_z=0.5 km. It is obvious that the 1-D velocity profiles at these different locations are not identical at 35 – 120 km depth due to the effect of random heterogeneity.

According to Frankel & Clayton (1986), the actual velocity fluctuations of heterogeneity in the 2-D von Karman type distribution in discrete random media cannot be simply described with σ since the standard deviation is undefined in such self-similar media. However, to discuss and compare the influence of such heterogeneity on surface-wave phase speeds among different heterogeneous models, we need to effectively describe the level of velocity fluctuation in the stochastic heterogeneity models. In this study, instead of applying the normalization with a converted standard deviation of heterogeneity strength for discrete media during the model construction (Frankel

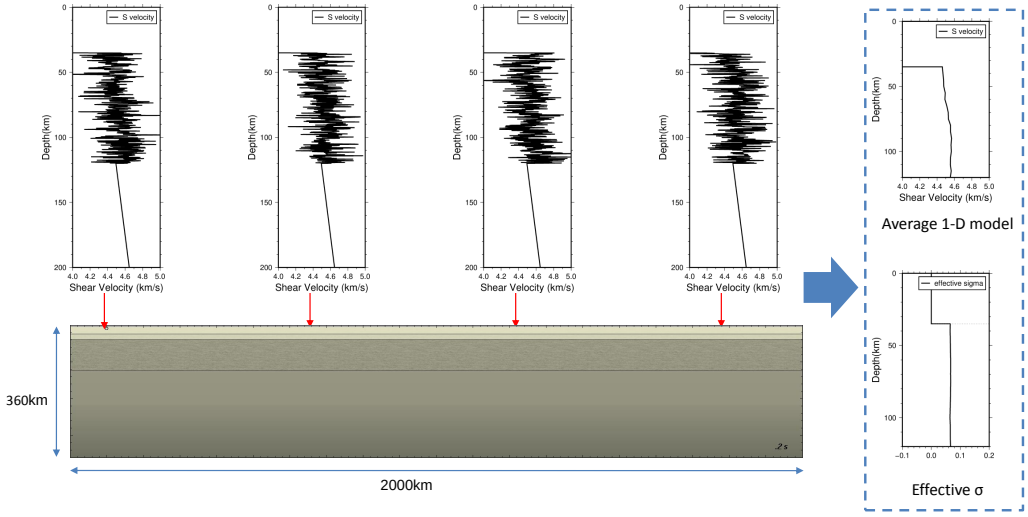

Figure 3.2: An example of averaged 1-D S-wave model and effective velocity fluctuation σ_{eff}. In this figure, heterogeneity with strength $\sigma = 0.05$, horizontal and vertical correlation length a_x=5 km, a_z=0.5 km is added to the 2-D homogeneous model in the 35 – 120 km depth. Selected 1-D velocity profiles for 4 different locations are shown on top. The average 1-D S-wave model and the corresponding effective strength of heterogeneity σ_{eff} computed from 200 different locations are shown on the right column.

& Clayton, 1986), we consider the effective velocity fluctuations in each heterogeneous model as follows.

We first calculated the average S-wave velocity at each depth in the 2-D heterogeneous model by using 200 1-D vertical profiles at every 10 km distance interval and obtained the average 1-D velocity profile. Then, at each depth, we computed the standard deviation of shear velocity. Both 1-D profiles of average velocity and standard deviations are then smoothed over a 10-km vertical window (5 km above and below the target depth), which is displayed in the right column of Fig. 3.2. The average value of these standard deviations over the heterogeneous layer can be considered as an *effective strength of velocity fluctuation*. We use a new variable σ_{eff} for this effective velocity fluctuation to distinguish it from the original σ presumed in the model construction. The relationship between σ and σ_{eff} for typical 2-D models used in this study is shown in Fig. 3.3.

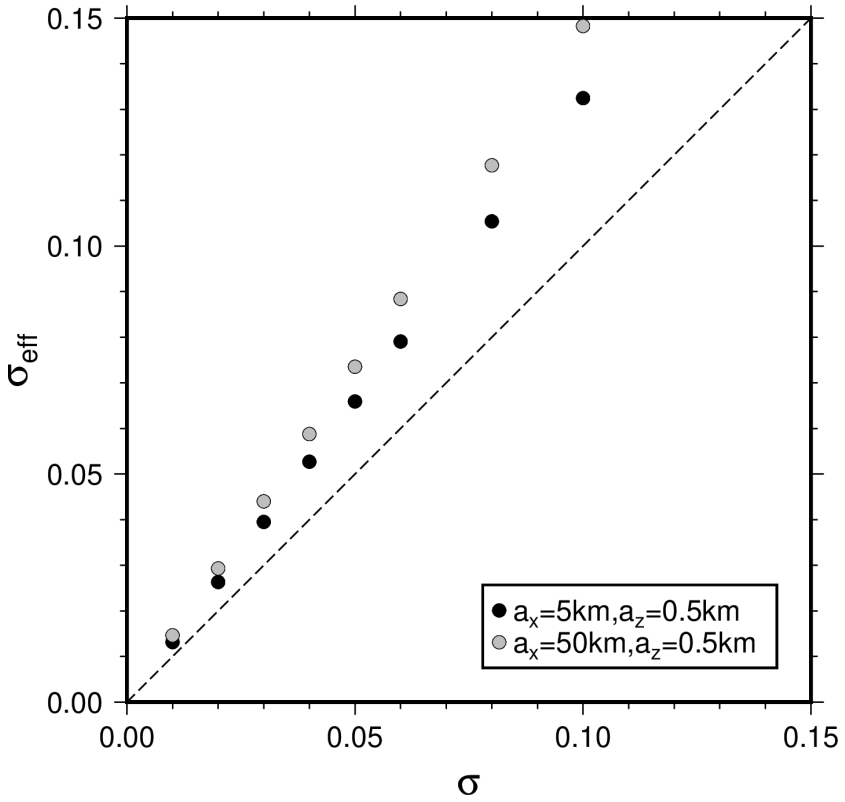

Figure 3.3: Relationship between original σ and its effective value σ_{eff} which is the standard deviation of velocity fluctuations in the actual 2-D models in the depth range of heterogeneous layer. The detail of computing σ_{eff} is explained in the main text.

3.1.2 Seismic wavefields and synthetic seismograms from the 2-D FDM simulations

We performed a series of 2-D forward modeling to numerically simulate the effect of laminated heterogeneities. Fig. 3.4 displays an example of a snapshot of P-SV wavefields in a 2-D heterogeneity model, and Figs. 3.5 and 3.6 displays the seismic record sections (vertical component) along a linear array of stations for higher (0.5–10Hz) and lower (0.01–0.03Hz) frequency ranges, respectively.

In the higher frequency range, we can clearly see the effects of fine-scale heterogeneity produces strong coda waves after the P and S waves, indicating the strong scattering effect as discussed in earlier studies (e.g., Kennett & Furumura, 2008). In the lower frequency range, very clear arrivals of surface waves (Rayleigh waves) can be traced. We can also see some artificial reflections from the sides and bottom of the 2-D structure domain, which may have some influence on surface waves. Such limitations of the 2-D waveform modeling will be further discussed in the next section.

The synthetic seismograms from the 2-D waveform modeling will be used in the subsequent sections to measure surface wave phase speeds in the longer-period range (30–100 s) displayed in Fig. 3.6, which will enable us to discuss the influence of laminated random heterogeneity on surface wave phase dispersion in Chapter 3.3 and apparent radial anisotropy in Chapter 4.

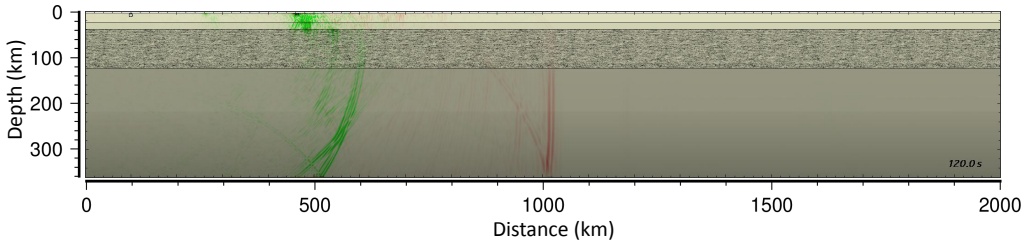

Figure 3.4: A snapshot of P-SV wavefield at an elapsed time of 120 s for a heterogeneous model (with heterogeneity parameters of $\sigma = 0.05$, $a_x = 5$ km, $a_z = 0.5$ km in the depth range from 35 to 120 km). P waves in red and SV waves in green.

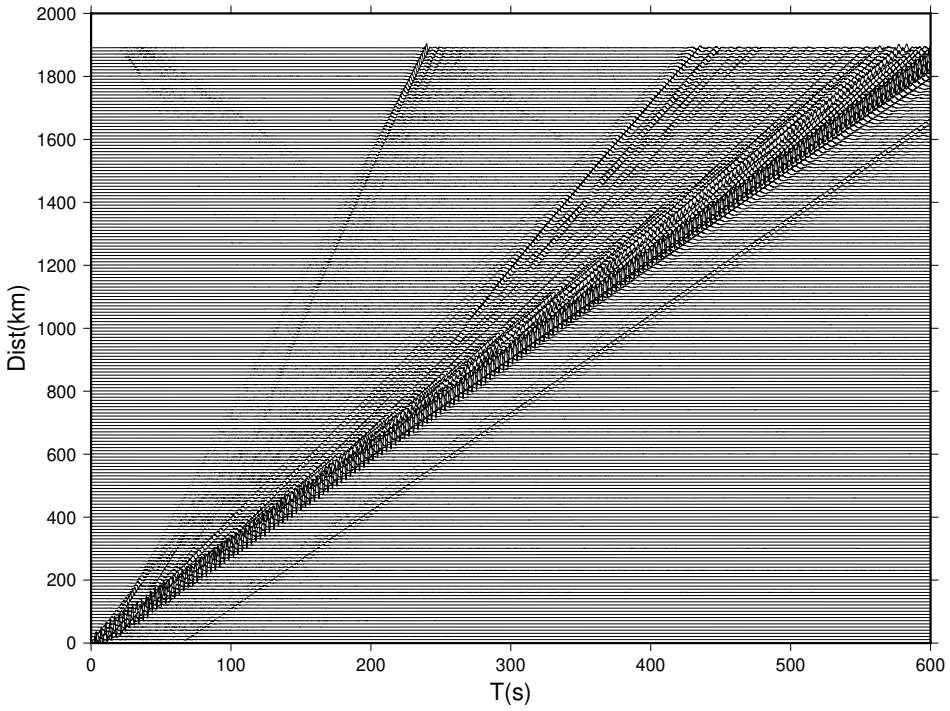

Figure 3.5: Vetical-component waveforms with a band-pass filter from 0.5 to 10 Hz, computed for the heterogeneous model shown in the snapshot of P-SV wavefield in Fig. 3.4.

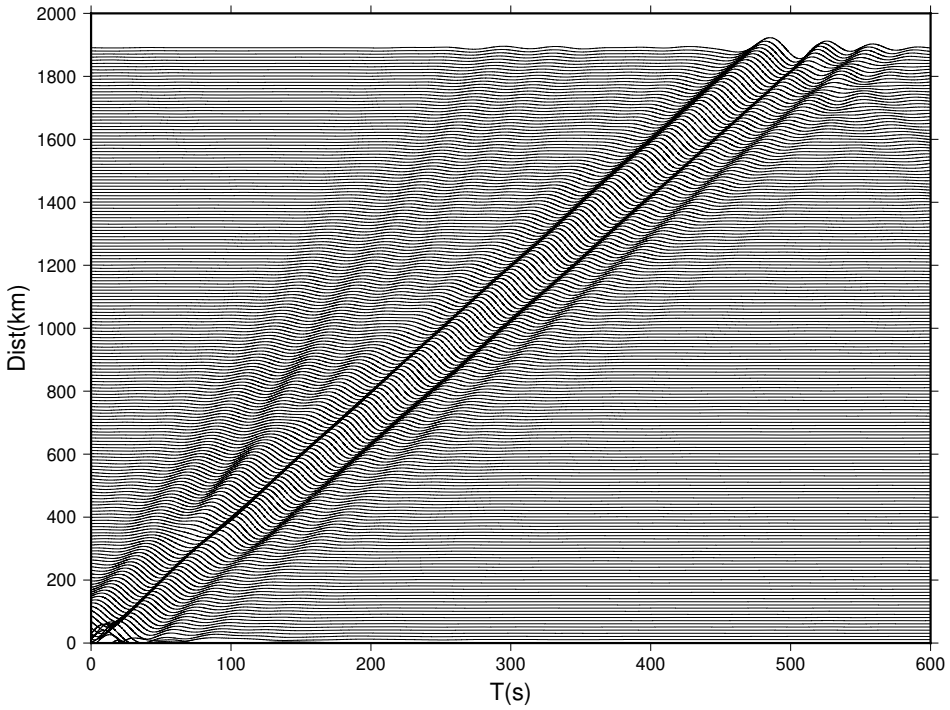

Figure 3.6: Same as Fig. 3.5 but with a band-pass filter from 0.01 to 0.03 Hz.

3.2 Phase speed measurements of surface waves

The main target of this study is to quantitatively estimate the influence of laminated random heterogeneity on long-period surface wave dispersion, which may eventually affect observed radial anisotropy. It is, therefore, necessary to estimate the surface-wave phase speeds from the simulated seismograms. In this study, we measure the phase speeds of fundamental-mode Rayleigh and Love waves based on the single-station measurements between the source and receivers based on a nonlinear waveform fitting method (Yoshizawa & Ekström, 2010), which enables us to measure phase speeds even at relatively short epicentral distances less than 2000 km in the current study. The details of the measurement procedure and the validity of the measured phase speed data sets are discussed in this section.

3.2.1 Single-station waveform fitting

In this study, we performed the nonlinear waveform fitting method for single-station phase speed measurements (Yoshizawa & Kennett, 2002; Yoshizawa & Ekström, 2010). This method inverts a single-station seismogram for path-specific 1-D profiles with a nonlinear model parameter search using the Neighbourhood Algorithm (Sambridge, 1999) to find a 1-D S-wave profile that provides the minimum misfit between the observed and synthetic seismograms. The best-fit 1-D profile can then be used to compute path-average multi-mode phase speeds for the source-receiver path. An example of the waveform fitting procedure and measured phase speeds are summarized in Fig. 3.7. We used the reliability parameter r_j (j is the mode number) defined by Yoshizawa & Ekström (2010) to evaluate the quality of waveform fitting. The threshold value for the fundamental mode is set to 10 in this study. The higher-mode amplitude is relatively weak in our numerical simulations since we assumed a shallow source at 5 km depth. Thus, we do not employ higher

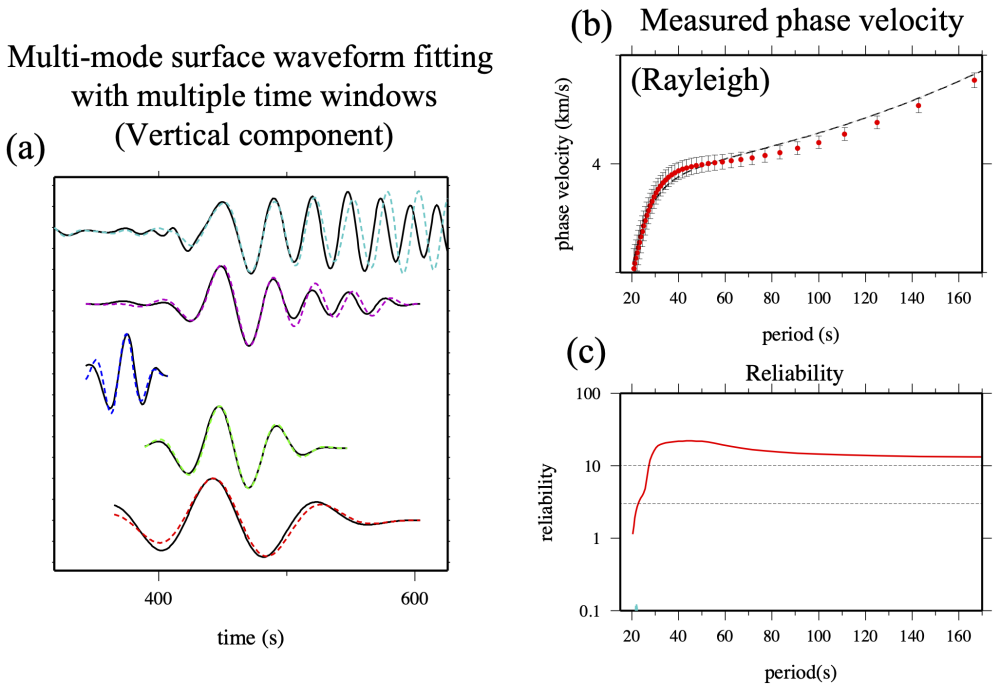

Figure 3.7: An example of single-station waveform fitting and phase speed measurements for Rayleigh waves. (a) Best-fit waveforms (color dashed lines) and observed waveforms (black lines; simulated seismograms in this study). (b) Measured phase speeds for the fundamental-mode Rayleigh waves. (c) Reliability parameters that represent the quality of measurements as a function of periods. Measured phase speeds with a reliability greater than 10 are used in the subsequent analysis.

modes in later processes and consider the fundamental mode only.

The 2-D models used in this study contain significant lateral variations of random heterogeneity. Therefore, we take the average of all measurements of single-station phase speeds for 101 stations distributed over a wide epicentral distance range (from 900 to 1900 km), so that we can discuss the average features of phase speed anomalies caused by the stochastic heterogeneity in each model. We also performed the dispersion measurements for simulated seismograms in a background homogeneous model without the stochastic random heterogeneity for comparison, which are then used as the

reference phase speed in the later process. The average phase speed perturbations computed for each heterogeneous model with respect to the common homogeneous background model enable us to discuss the influence of the random heterogeneity on surface wave dispersion. Note that we employed high-quality measurements of phase speeds with a reliability parameter r_0 >10.0 in this averaging process.

3.2.2 Quality check of phase speed measurements

Homogeneous layered model

A homogeneous layered model includes no lateral variation, so we can use the background 2-D layered model (equivalent to a 1-D velocity structure) to compute theoretical phase speeds for Rayleigh and Love waves based on the normal-mode method with MINEOS (Masters et al., 2011). Note that the 2-D model used in this study does not have structural information below 360 km depth, so the deep structure below 360 km is added by using iasp91 and PREM, following the description in Chapter 3.1.1. The comparisons between the measured phase speeds from simulated seismograms and those from the normal-mode theory are shown in Fig. 3.8 for both Rayleigh (P-SV) waves and Love (SH) waves.

Measured phase speeds for the fundamental-mode Rayleigh waves from the single-station method (Fig. 3.8 a) exhibit smaller errors in the period range from 30 – 60 s, matching well with the theoretical phase speeds for the 1-D background model from the normal mode theory. In a longer period, the single-station phase speeds become slower than the theoretical ones due to the limited model space in the 2-D simulation, which includes only the top 360 km, while the full Earth model is used in the normal mode calculation, which includes faster S velocity below 360 km depth. Also, the epicentral distance range (900 – 1900 km) used in our phase speed measurements is

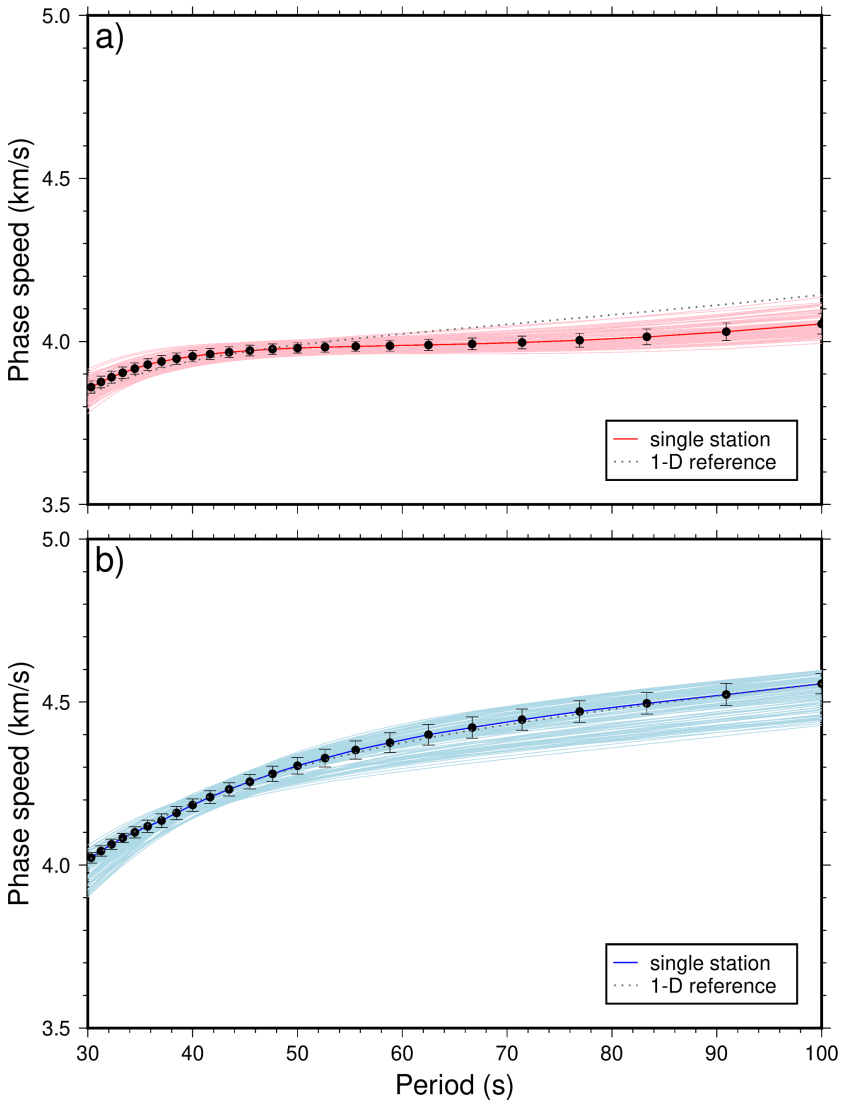

Figure 3.8: Dispersion curves for the fundamental-mode surface wave phase speeds in the homogeneous model measured by the single-station waveform fitting. (a) Rayleigh wave phase dispersion curves. Thin red lines: single-station measurements for 101 stations. A thick red line: ensemble average of 101 stations using selected measurements with higher reliability parameter r_0 >10. Error bars are the standard deviations at each period. Grey dotted line: the theoretical phase dispersion curve computed from the background 2-D homogeneous model (1-D profile) using the normal-mode theory. (b) Same as (a) but for Love wave with blue lines.

relatively short compared to the wavelength of surface waves at 100 s (over 400 km wavelength), which also makes the measurements somewhat unstable in the longer period. Thus, the standard deviation of measurements tends to be greater in the longer period range.

For the Love wave case (Fig. 3.8 b), the average phase speeds from the single-station measurements are almost equal to the theoretical phase speeds from the normal-mode calculation since the fundamental-mode Love waves are essentially less sensitive to the structure below 360 km in the current period range (30 – 100 s). Still, the standard deviations of Love wave phase speeds tend to be larger than those of Rayleigh waves. This can be attributed to the well-known contamination of the fundamental-mode Love waves (at relatively short epicentral distances) by the preceding body waves (such as multiply reverberated S waves) and higher modes (e.g., Nettles & Dziewoński, 2008; Foster et al., 2014; Matsuzawa & Yoshizawa, 2019), since the higher-modes and fundamental-mode share similar group speeds. Despite such limitations, we could extract the stable average phase speeds by taking the average of all the reliable measurements, which is very close to the theoretical velocities in the period range of 30 – 100 s.

Heterogeneous layered model

Now we consider our main target of 2-D models with random heterogeneities. Here we performed FDM simulations for heterogeneous models incorporating stochastic laminated heterogeneity with the strength of heterogeneity $\sigma = 0.1$ ($\sigma_{eff} = 0.132$), the horizontal correlation length $a_x = 5$ km and the vertical correlation length $a_z = 0.5$ km in the depth range of 35–120 km. Fig. 3.9 compares the average phase dispersion curves measured from the single-station method using the simulated seismograms for the heterogeneous and homogeneous background models.

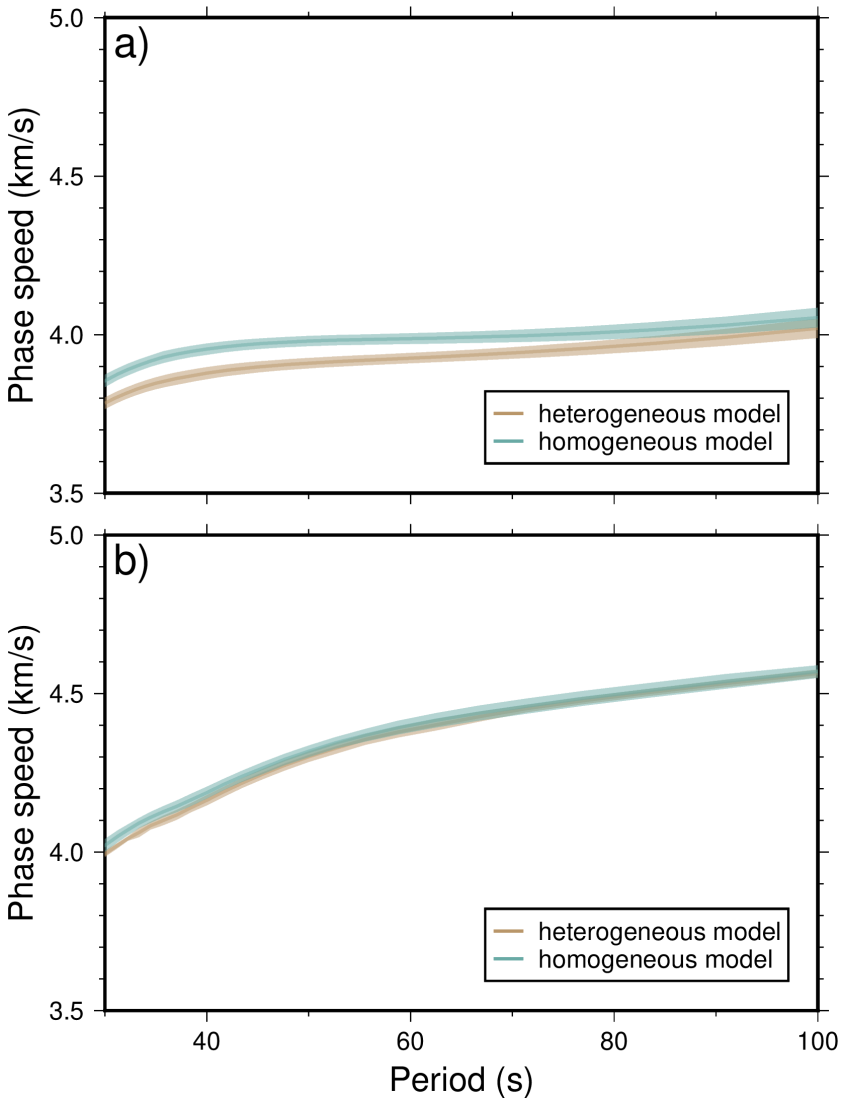

Figure 3.9: Average phase dispersion curves of (a) Rayleigh wave and (b) Love wave, measured with the single-station method using the simulated seismograms for the heterogeneous model (brown) and for the homogeneous model (green) shown in Fig. 3.8. Colored envelopes show the standard deviation of all measurements with reliability r_0 >10.

For Rayleigh waves (Fig. 3.9 a), we can see apparent differences in the average phase speeds between the heterogeneous and homogeneous models, especially in the shorter period range (30 – 70 s), which represents the influence of laminated random heterogeneity. This discrepancy becomes smaller in the longer periods since the depth range of stochastic heterogeneity in our model is confined in the depth range of 35 – 120 km. The standard deviations (colored envelopes in Fig. 3.9) of phase speed measurements from the heterogeneous model are generally at the same level as the homogeneous case, indicating that the quality of phase speed measurements has been unaffected even in the heterogeneous models.

For Love waves (Fig. 3.9 b), the difference between the average phase speeds for the heterogeneous model and the homogeneous model is very small. As discussed in Chapter 2, the effective shear modulus for a horizontally polarized SH wave can be derived from the arithmetic average of the horizontally layered model over depth, which is equivalent to the homogeneous background model. Thus, the horizontally laminated random heterogeneity should have little impact on the Love wave phase speed on average. Therefore, in the subsequent sections, our discussion mainly focuses on the phase speed changes of Rayleigh waves in the 2-D random models, which eventually represent the structure-induced apparent radial anisotropy that will be treated in Chapter 4.

It should be noted that the velocity structure of the heterogeneous model can be affected by the specific random seeds used for generating stochastic heterogeneity during the model construction. Fig. 3.10 shows the average phase speeds of Rayleigh wave for 5 different heterogeneous models with different random seeds, using the same model parameter sets used in Fig. 3.9. The variations between models with different random seeds are relatively small but may need to be carefully considered when we discuss the structural

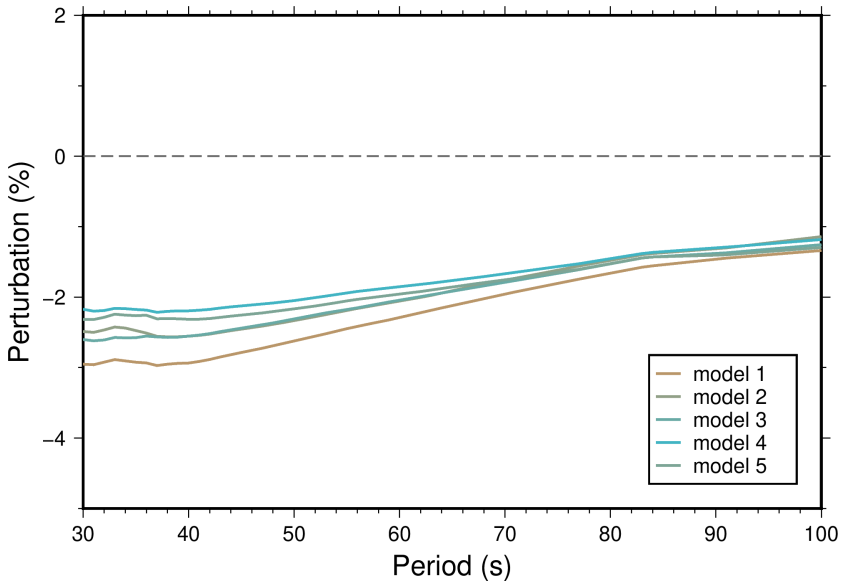

Figure 3.10: Average phase speed perturbations of Rayleigh waves for the heterogeneous models (measured with the single-station methods) relative to the average phase speed for the homogeneous models. Laminated heterogeneities with the standard deviation σ=0.1 (σ_{eff} = 0.132) are imposed in the depth range between 35 – 120 km, with the horizontal and vertical correlation lengths a_x = 5 km and a_z = 0.5 km, respectively. Colored lines: Average phase speed perturbations estimated from each of 5 models with different random seeds, using measured phase speeds with the reliability r_0 >10.

influence on surface wave dispersion.

Fig. 3.11 displays 1-D profiles of average S-wave models and the corresponding effective velocity fluctuations σ_{eff} for each case of 5 different random-seed models. The σ_{eff} is essentially the same for all models, but the average S-wave profile tends to show slight differences, which may have more impact than σ_{eff} on the differences of phase speed perturbations shown in Fig. 3.10.

Fig. 3.12 shows the ensemble average of the Rayleigh wave phase speed perturbations for 5 different random-seed models shown in Fig. 3.10. All of the average phase speeds for each random seed model are within the range of

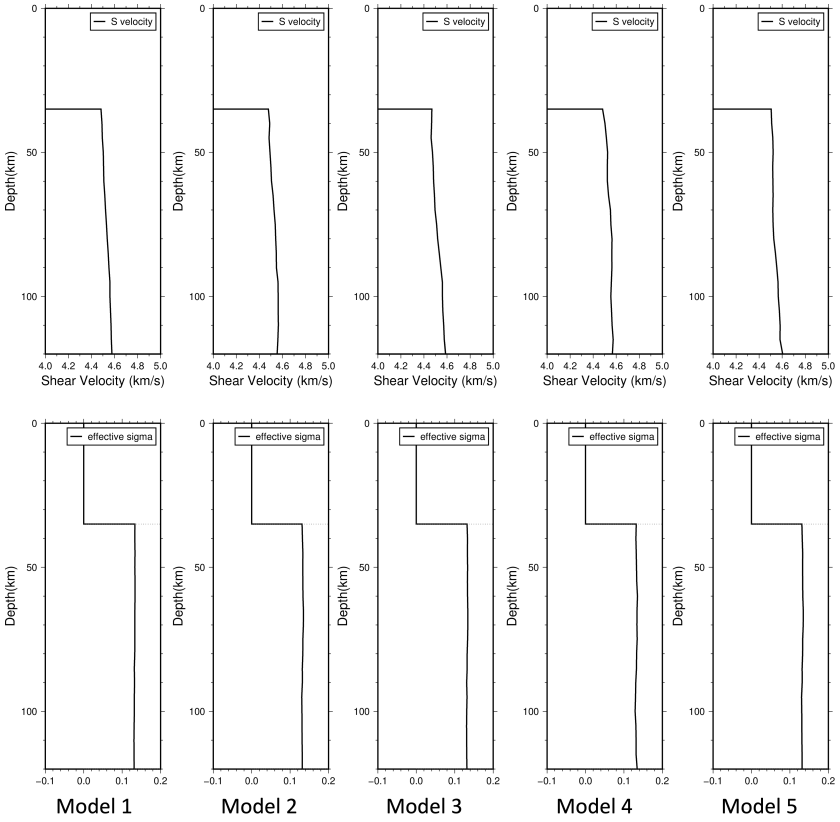

Figure 3.11: Vertically-smoothed average 1-D S-wave models and effective velocity fluctuations σ_{eff} for 5 random models used in Fig. 3.10 with different random seeds. Top: average 1-D S-wave model calculated from 1-D vertical profiles at various locations. Bottom: corresponding σ_{eff} for the heterogeneity in the depth range of 35–120 km.

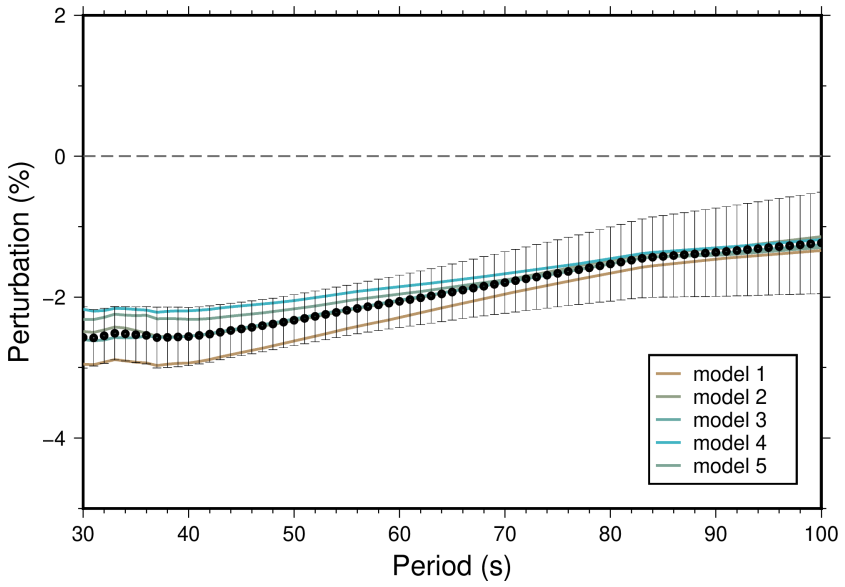

Figure 3.12: Same as Fig. 3.10, but also shows the average values and standard deviations calculated from 5 different random-seed models (black dots and error bars).

the standard deviation of the ensemble phase speed perturbations. Thus, the ensemble-averaged phase-velocity perturbations from 5 random-seed models can be a good representation of the mean feature of the heterogeneity model with the specific model parameter sets ($a_x = 5$ km, $a_z = 0.5$ km, and $\sigma = 0.1$ in this case). It may be better to use more different random seed models, but it is prohibitive considering the computational costs. In the subsequent sections, unless otherwise specified, phase speeds and their perturbations from the homogeneous models are the ensemble average value from 5 distinct models with identical parameter sets, but with different random seeds, to suppress the uncertainties in the random models.

3.2.3 Numerical effects and limitations in the 2-D FDM simulations

In the previous sections, we investigated the validity of synthetic seismograms from the 2-D FDM simulations and the measured phase speeds using those

seismograms with the single-station waveform fitting. When we use this kind of numerical approach for surface wave modeling and analysis, we cannot avoid the intrinsic numerical limitations, such as the free-surface treatment, a half-grid shift in the staggered grid, numerical dispersion, and absorbing boundary conditions (e.g., Igel, 2016). In fact, the absorbing boundary at both sides and bottom of the 2-D model cannot perfectly eliminate boundary reflections, as shown in the waveform traces in Figs. 3.5 and 3.6, which would have some influence on our synthetic seismograms.

Moreover, in this study, we have to limit the model space to 2000 km horizontally and 360 km vertically, which is a relatively small size for the propagation of long-period surface waves. This requirement is due to the practical limit of computational resources to incorporate very small grids of 0.05 km to properly model the fine-scale laminated heterogeneity. The 2-D flat models used in this study require a proper treatment of Earth flattening corrections, which have been handled properly within the limited depth range. Such limited model size may affect the absolute Rayleigh wave phase speeds to some extent, as we have discussed in the previous section.

However, all the above numerical issues can be assumed to be common in all of our simulated seismograms for both 2-D heterogeneous and homogeneous models. Therefore, by taking the difference between the phase speeds measured for the heterogeneous and homogeneous models, the majority of the intrinsic numerical effects can be canceled out. Thus, we can extract robust information on surface wave phase speed changes due to the laminated random heterogeneity. This assumption will be employed in the subsequent sections, and we will discuss the phase speed perturbations in heterogeneous media relative to the average phase speed in the homogeneous model.

3.3 Phase speed anomalies caused by laminated random heterogeneity

In this section, we discuss the effect of laminated heterogeneity with various parameter sets for stochastic random media on the surface-wave phase dispersion based on the phase speed measurements using the methods described in the previous section.

3.3.1 Effects of the strength of heterogeneity

We considered a series of 2-D simulations with the same heterogeneity parameter sets ($a_x = 5$ km, $a_z = 0.5$ km) except for the strength of heterogeneity σ, varying from 0.01 to 0.1 (Fig. 3.13 and Table 3.1). The resultant phase speed perturbations from the average phase speeds in the homogeneous model are shown in Fig. 3.14 for Rayleigh waves and Fig. 3.15 for Love waves.

We can clearly see that larger σ causes larger negative phase speed perturbations for the fundamental-mode Rayleigh waves, while the difference for Love waves are not very significant. The case with σ=0.1 ($\sigma_{eff} \approx 0.13$, equivalent to S-wave velocity fluctuations of about $\pm$ 13 %) resulted in a largest phase speed perturbation of about 2 – 2.5 % velocity drop for the fundamental-mode Rayleigh wave at 30 – 60 s period, relative to the homogeneous case (no heterogeneity in all layers). Although such a very strong

	Depth range	a_x	a_z	σ	σ_{eff}
Model 1	35 – 120 km	5 km	0.5 km	0.01	0.0131
Model 2	35 – 120 km	5 km	0.5 km	0.02	0.263
Model 3	35 – 120 km	5 km	0.5 km	0.05	0.659
Model 4	35 – 120 km	5 km	0.5 km	0.10	0.132

Table 3.1: Model parameters for stochastic random heterogeneity with fixed a_x and a_z, and varying σ used in Figs. 3.13 – 3.15.

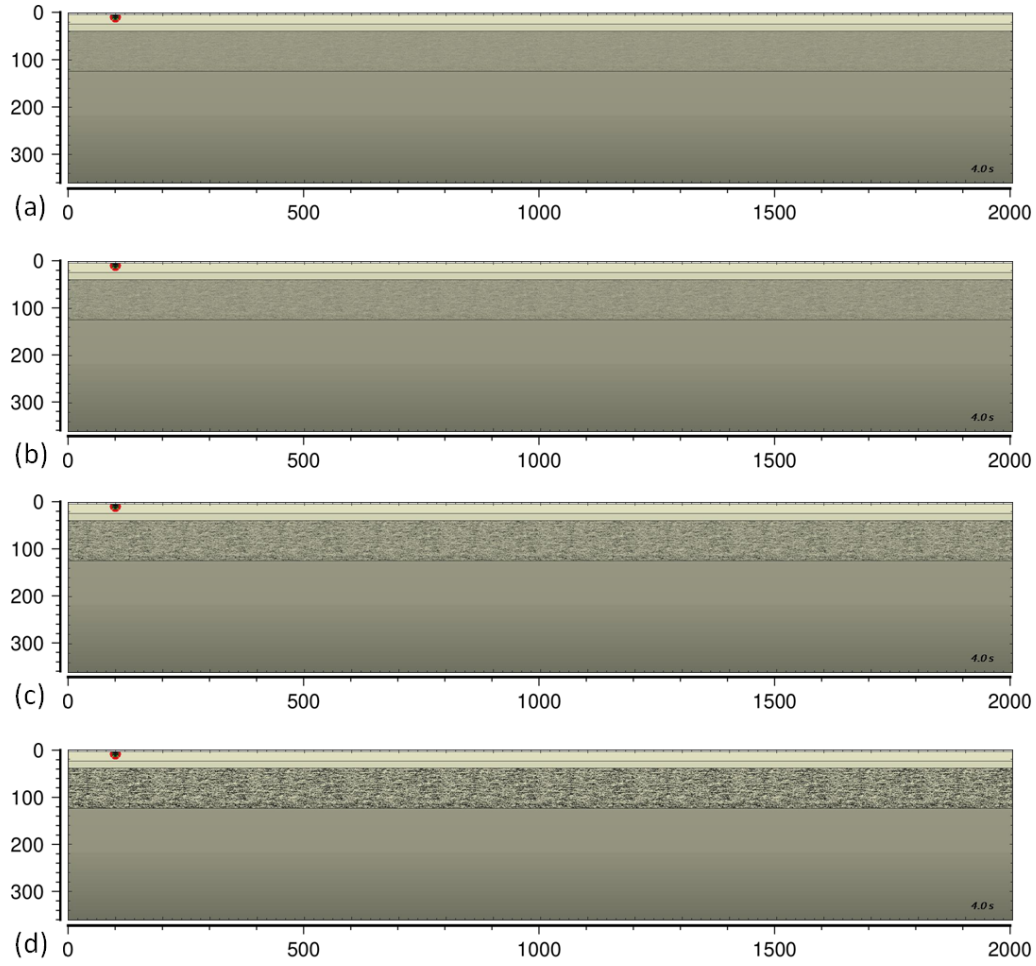

Figure 3.13: Examples of 2-D heterogeneous models used to estimate average phase speeds in Figs. 3.14 and 3.15. Laminated heterogeneities are confined in the depth range between 35 – 120 km, and horizontal and vertical correlation lengths are fixed with $a_x = 5$ km and $a_z = 0.5$ km, respectively. The strengths of heterogeneity σ are (a) $\sigma = 0.01$, (b) $\sigma = 0.02$, (c) $\sigma = 0.05$, and (d) $\sigma = 0.10$.

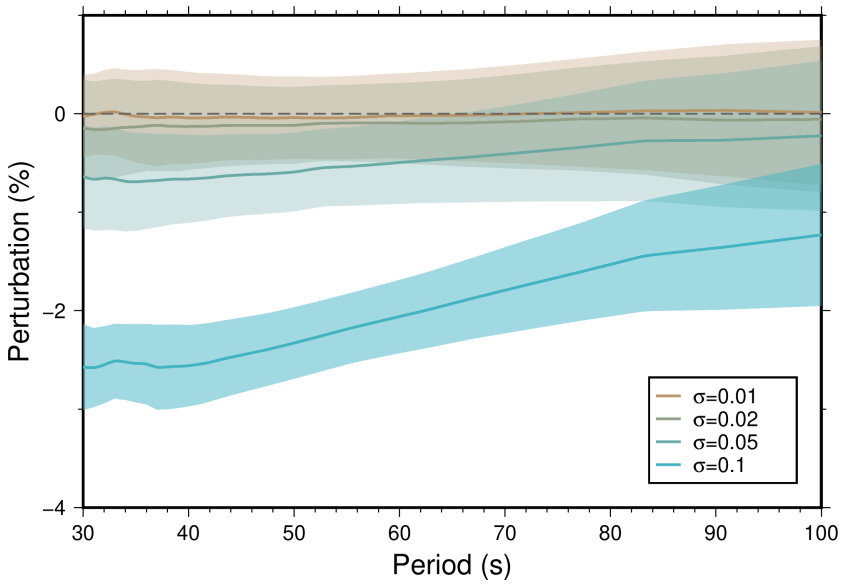

Figure 3.14: Average phase speed perturbations for the fundamental-mode Rayleigh wave relative to the average phase speed in the homogeneous model (a dashed horizontal line at 0 %), estimated from the ensemble average of single-station measurements (with reliability parameter r_0 >10). The standard deviation from the ensemble average of measurements is calculated and displayed as colored envelopes around the average. The horizontal and vertical correlation lengths are fixed (a_x = 5 km, a_z = 0.5 km), while σ varies from 0.01 to 0.1. Laminated random heterogeneities are confined in the depth range between 35 and 120 km of the 2-D model as shown in Fig. 3.13.

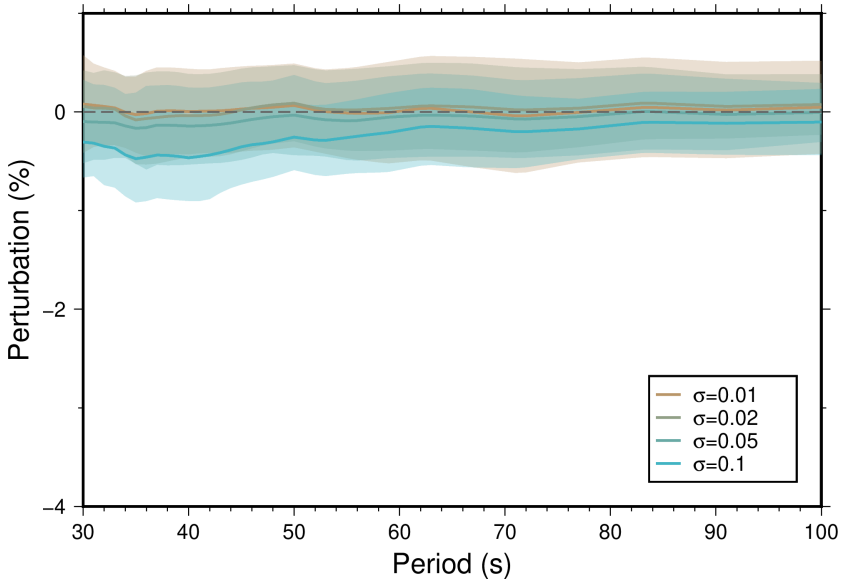

Figure 3.15: Same as Fig. 3.14 but for Love wave.

heterogeneity may locally exist in certain areas of the Earth, it may be somewhat unlikely to occur continuously over a large horizontal scale (>1000 km). Still, even in a more practical case with σ=0.05 ($\sigma_{eff} \approx 0.066$), we can see non-negligible influences of such heterogeneity on Rayleigh wave phase speeds, which drops about 0.6 % in a period range of 30 – 55 s.

Earlier studies on scattering of higher-frequency body waves in a stochastic heterogeneity prefer relatively smaller values for σ since the observations of high-frequency body waves or P wave reflectivity suggest that the realistic fluctuation would be about 2 % or even smaller (Kennett, 2015). However, the laminated heterogeneity with $\sigma = 0.02$ ($\sigma_{eff} \approx 0.026$) only shows mild phase speed deviations (about 0.2 %) for the fundamental-mode Rayleigh waves. Another case with σ=0.01 ($\sigma_{eff} \approx 0.013$) shows almost no difference in the wide period range, suggesting that the weak laminated heterogeneity has essentially no influence on the long-period surface waves.

Fig. 3.16 is a summary diagram showing the relationship between the average phase speed perturbation and the effective strength of heterogeneity

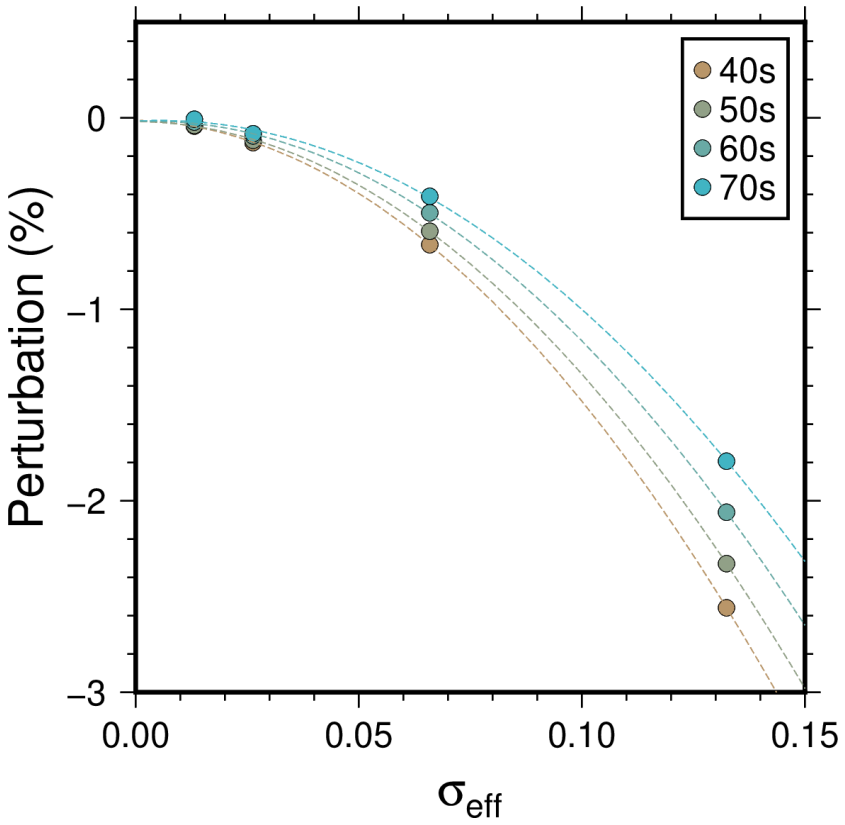

Figure 3.16: Average phase speed perturbations for Rayleigh waves relative to the homogeneous model as a function of effective velocity fluctuations σ_{eff} (colored dots) for four periods from 40 to 70 s. The relationship between σ and σ_{eff} is shown in Fig. 3.3. Dashed lines are the best-fit curve for each period, using a second-order (quadratic) polynomial.

σ_{eff}. Although we have only four selected samples, the relationship between these two parameters is clearly not on a linear trend, as the phase speed perturbation changes rapidly with increasing σ_{eff}.

3.3.2 Effects of the horizontal correlation length of heterogeneity

Here we consider the effect of varying horizontal correlation length a_x, which controls the characteristic horizontal size of heterogeneity. Since our main target is to consider the elongated (finely layered) random heterogeneity, we consider stochastic heterogeneity with fixed vertical correlation length a_z (= 0.5 km), representing the varying aspect ratios of heterogeneity (Fig. 3.17). Stochastic model parameter sets with varying a_x used in this section are summarized in Table 3.2. Note that, in this case, the effective velocity fluctuations σ_{eff} tend to be greater as a_x becomes large (see, Fig. 3.3 and Table 3.2), which needs to be considered in the following discussion.

Average phase speed perturbations from models with varying a_x are shown in Fig. 3.18 for the Rayleigh wave and Fig. 3.19 for the Love wave. We used 3 different values for a_x from medium scale (a_x = 50 km) to fine-scale isotropic heterogeneity ($a_x = a_z$ = 0.5 km). As in the previous example of varying σ, Love waves are essentially less affected even in this case. The varying a_x exhibits a stronger influence on the phase speed perturbation of the fundamental-mode Rayleigh wave for larger a_x. This is partly because the effective velocity fluctuations σ_{eff} becomes greater for larger a_x as in Table 3.2.

To distinguish the effects of correlation length a_x from the varying ef-

	Depth range	a_x	a_z	σ	σ_{eff}
Model 1	35 – 120 km	0.5 km	0.5 km	0.05	0.0548
Model 2	35 – 120 km	5 km	0.5 km	0.05	0.0659
Model 3	35 – 120 km	50 km	0.5 km	0.05	0.0736

Table 3.2: Model parameters for random heterogeneity with fixed a_z and σ, and varying a_x used in Figs. 3.17 – 3.19.

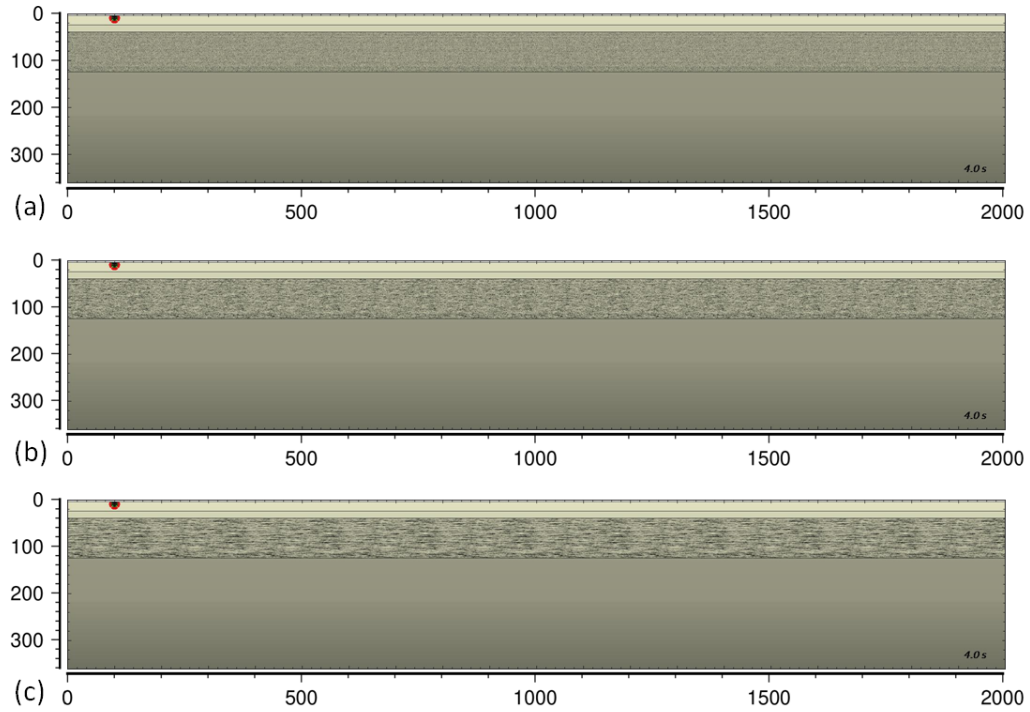

Figure 3.17: Examples of 2-D heterogeneous models used to estimate average phase speeds in Figs. 3.18 and 3.19. Laminated heterogeneities are confined in the depth range between 35 – 120 km, with fixed parameters of the vertical correlation length $a_z = 0.5$ km and the strength of heterogeneity $\sigma = 0.05$. The horizontal correlation lengths a_x are (a) 0.5 km, (b) 5 km, and (c) 50 km.

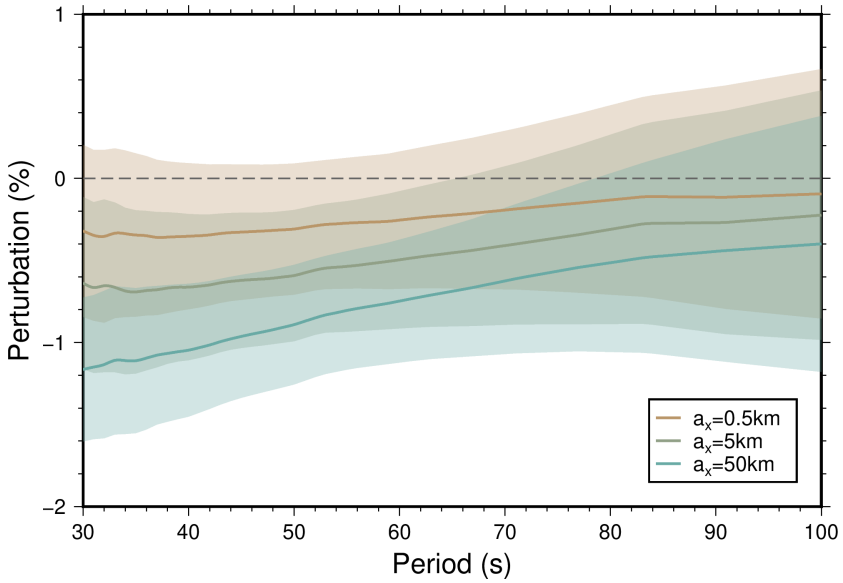

Figure 3.18: Same as Fig. 3.14 (average phase speed perturbations for the Rayleigh wave, relative to the homogeneous model), but for the 2-D models in Fig. 3.17 with fixed $a_z = 0.5$ km and $\sigma = 0.05$, and varying a_x from 0.5 to 50 km.

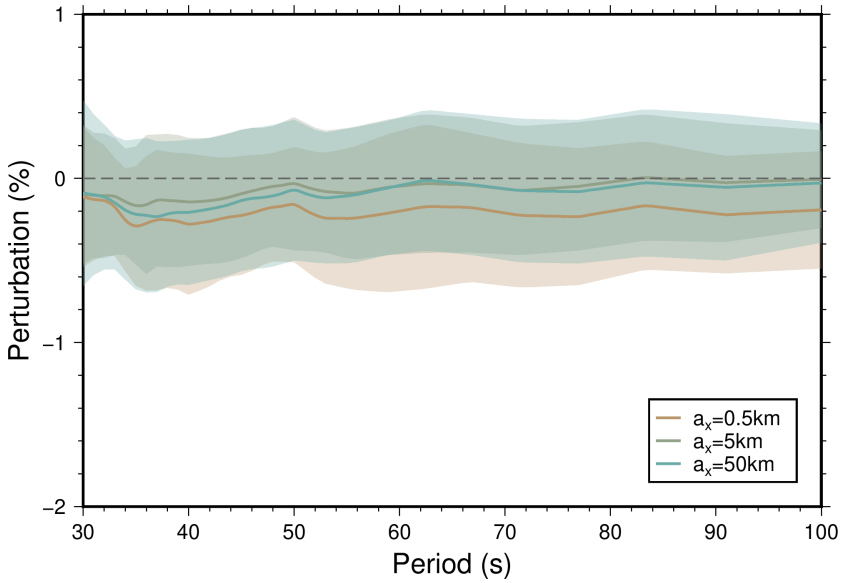

Figure 3.19: Same as Fig. 3.18 but for the Love wave.

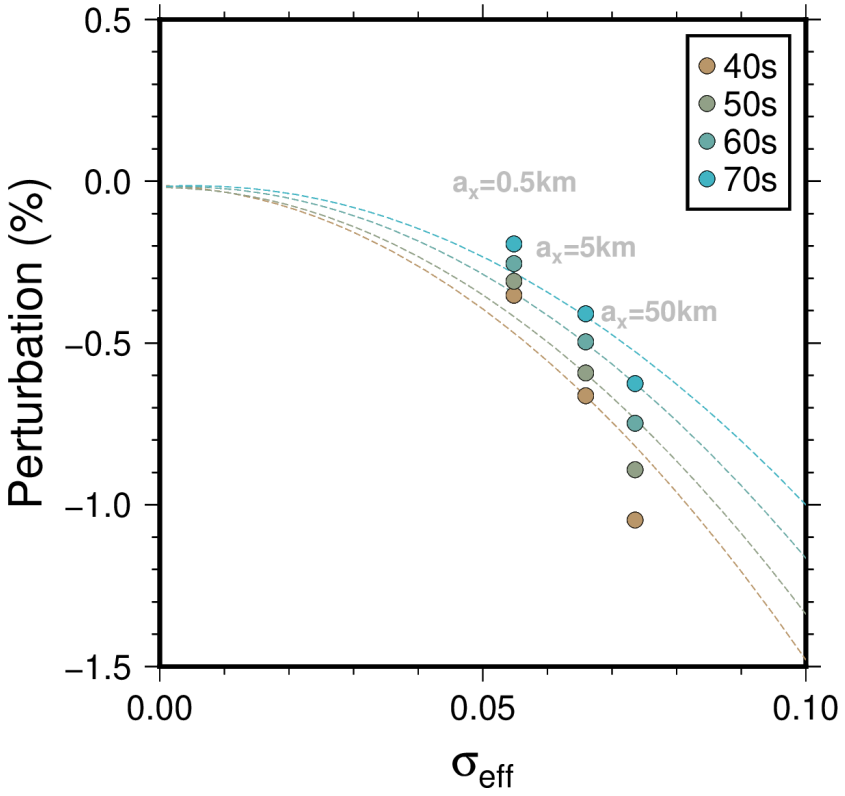

Figure 3.20: Same as Fig. 3.16 but for varying a_x. Dashed lines show the best fit curves with the varying σ_{eff} case shown in Fig. 3.16

fective velocity fluctuations σ_{eff}, we consider the diagram of average phase speed perturbation as a function of σ_{eff} in Fig. 3.20. Considering the relative differences from the best-fit curves derived from the previous experiments in section 3.3.1 for fixed a_x (= 5 km) and a_z (= 0.5 km), we can discuss the realistic influence of varying a_x on the phase speed perturbation of Rayleigh waves. Although our current sample is only limited to three cases, we can see that as the a_x becomes greater, the average phase speed perturbations of Rayleigh waves tend to be slower (Fig. 3.20).

3.3.3 Effects of the thickness of heterogeneous layer

The thickness of the heterogeneous layer in the lithosphere is another property to be considered in our model. To simplify the problem, here we consider 2-D models in which the laminated stochastic heterogeneity exists throughout the lithosphere with varying thickness. In the actual Earth, the lithosphere thickness varies from place to place. Stable Archean and Proterozoic cratons generally have thick lithosphere over 200 km (e.g., Yuan & Romanowicz, 2010; Yoshizawa, 2014), while the lithosphere under the Phanerozoic basements (e.g., in eastern Australia) tends to be thinner than 100 km (e.g., Fishwick et al., 2008; Yoshizawa, 2014). Kennett et al. (2013) have also used several different models with varying lithosphere thickness to investigate its influence, although they focused on the oceanic region with a very thin crust and lithospheric mantle (<100 km).

Here we primarily consider the continental case with a fixed crustal thickness of 35 km, with varying thickness of lithosphere between 100 km (representing thinner lithosphere equivalent to the relatively young continental area) and 250 km (representing thick lithosphere in stable continental regions or cratons). Such spatial variations of the lithosphere thickness can be commonly observed in a large single continent (e.g., in Australia, North

	Depth range	a_x	a_z	σ	σ_{eff}
Model 1	35 – 100 km	5 km	0.5 km	0.05	0.0659
Model 2	35 – 150 km	5 km	0.5 km	0.05	0.0659
Model 3	35 – 200 km	5 km	0.5 km	0.05	0.0659
Model 4	35 – 250 km	5 km	0.5 km	0.05	0.0659

Table 3.3: Model parameters for stochastic random heterogeneity with fixed σ, a_x and a_z with varying depth range of heterogeneous layer used in Figs. 3.21 – 3.23.

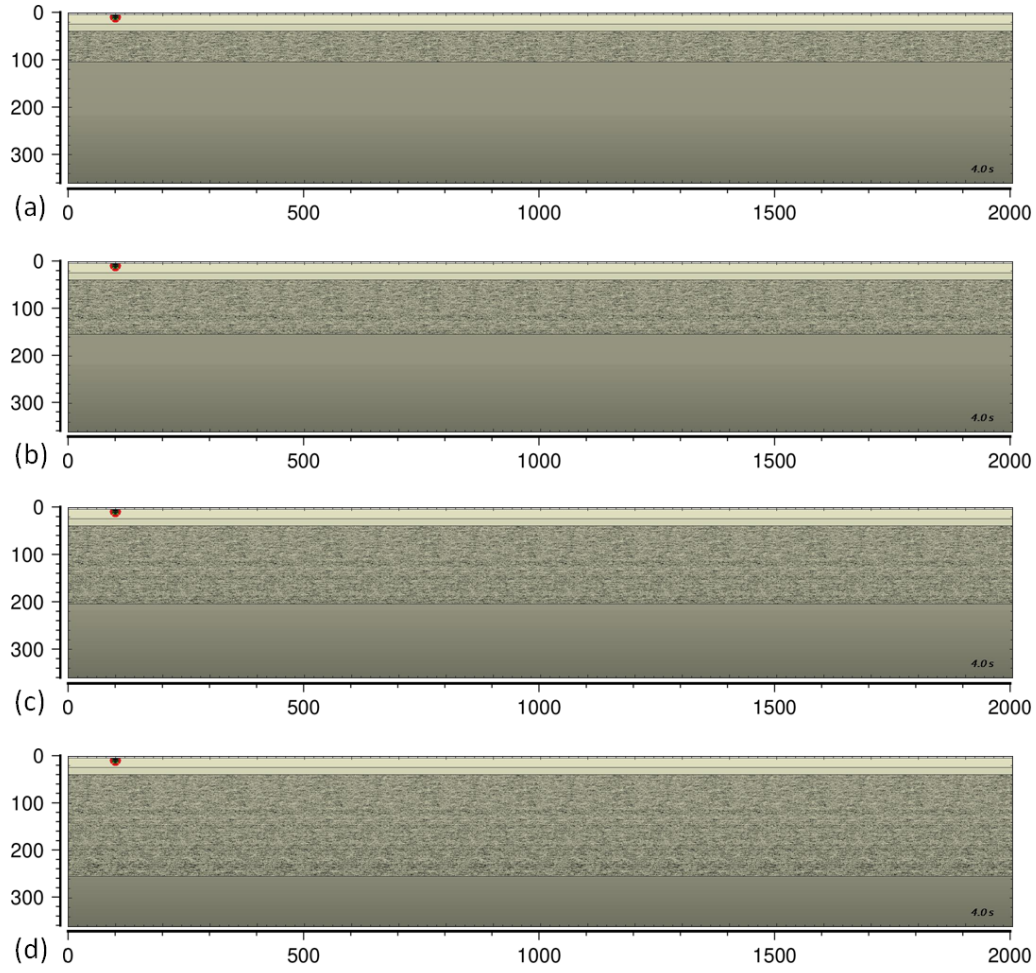

Figure 3.21: Example of 2-D heterogeneous models used to estimate average phase speeds in Fig. 3.22 for the Rayleigh wave and Fig. 3.23 for the Love wave, with the varying thickness of the heterogeneous layer. Three parameters to control the laminated heterogeneity (i.e., a_x, a_z, and σ) are fixed as $a_x = 5$ km, $a_z = 0.5$ km, and $\sigma = 0.05$. The depth ranges of laminated heterogeneities are (a) 35 – 100 km, (b) 35 – 150 km, (c) 35 – 200 km, and (d) 35 – 250 km.

America, etc).

Fig. 3.21 displays the laminated heterogeneous models with varying thicknesses of the heterogeneous layer. Fig. 3.22 and Fig. 3.23 show the phase speed perturbations of the fundamental-mode Rayleigh and Love waves, respectively, for the models in Fig. 3.21. The employed stochastic parameters are summarized in Table 3.3.

The phase speed perturbations of Rayleigh waves in the longer period gradually increase as the heterogeneous layer becomes thicker, while those in the shorter period are similar. In the period shorter than 50 s, all models exhibit similar phase speed perturbations as the fundamental-mode Rayleigh wave in this period range are mostly sensitive to the shallow structure above 80 km, where all of the 2-D models in Fig. 3.21 includes the stochastic heterogeneity. Longer-period Rayleigh waves are more sensitive to the deeper structure below 100 km, where some of the models do not include stochastic heterogeneity. Meanwhile, the Love-wave phase speed perturbations are not very significant also in this case, with nearly the same patterns of velocity perturbations for all cases of the varying thickness of the heterogeneous layer. These results suggest that the effects of varying thicknesses of the heterogeneous layer on phase speed perturbations mostly reflect the vertical sensitivity of Rayleigh waves as a function of periods.

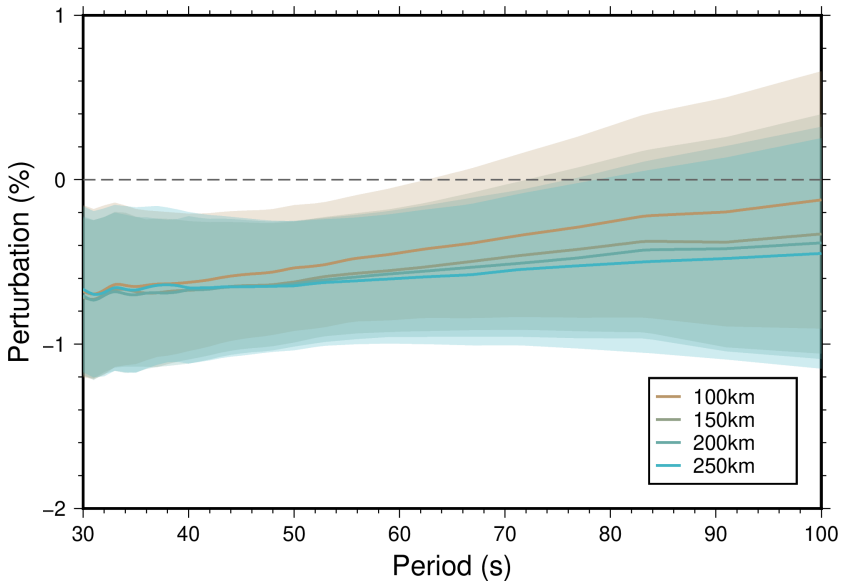

Figure 3.22: Same as Fig. 3.14 (average phase speed perturbations for the Rayleigh wave, relative to the homogeneous model), but for the models in Fig. 3.21 with varying thickness of the heterogeneous layer. The thickness of the heterogeneous lithosphere varies from 35 – 100 km to 35 – 250 km, while other parameters are fixed ($\sigma = 0.05$, $a_z = 0.5$ km, and $a_x = 5$ km).

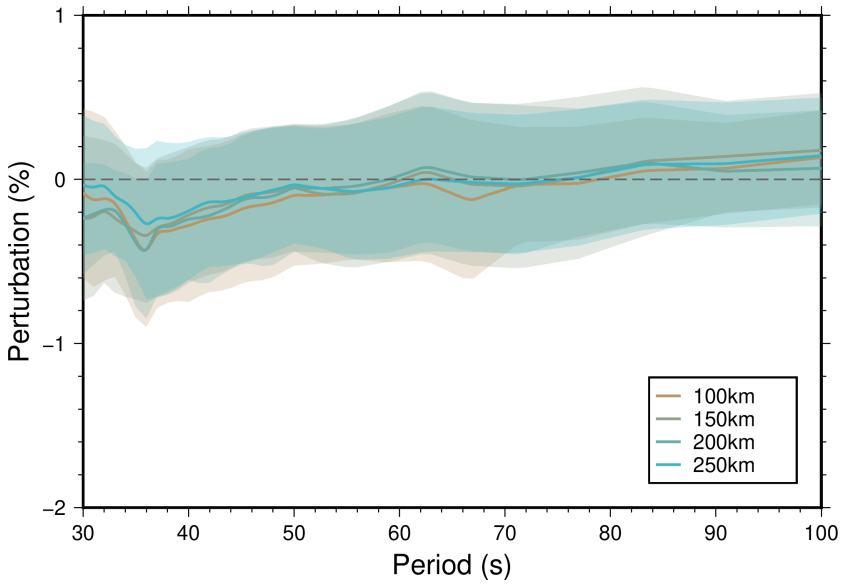

Figure 3.23: Same as Fig. 3.22 but for the Love wave.

Chapter 4

Estimation of apparent radial anisotropy induced by laminated heterogeneity

In the previous chapter, we measured the average phase speeds for the fundamental-mode Rayleigh and Love waves for 2-D heterogeneity models and calculated the perturbations from the homogeneous case to discuss the effects of stochastic heterogeneity on surface wave dispersion. These phase speed perturbations caused by the stochastic distributions of laminated heterogeneity indicate apparent radial anisotropy generated from the quasi-layered structure. To investigate the direct link of such phase speed perturbations with the radial anisotropy, we invert the estimated phase speed perturbations for 1-D shear wave models, including both SV and SH waves.

4.1 Inversions for radially anisotropic S wave models

4.1.1 Method of inversions

In this study, the average single-station phase speeds for both Rayleigh and Love waves in a period range from 30 to 100 s are simultaneously inverted for 1-D V_{SV} and V_{SH} models using an iterative non-linear least-square inversion method by Tarantola & Valette (1982). The practical application of this inversion method for radially anisotropic S wave models has been described in detail by Yoshizawa (2002) and Yoshizawa (2014).

In this study, we consider the set of six model parameters (ρ, α_H, α_V, β_V, β_H, η), where ρ is density, α_H and α_V are PH and PV wave velocities, β_V and β_H are SV and SH wave velocities, and η is the dimensionless anisotropic parameter. Following Yoshizawa (2014), β_V and β_H are used as independent model parameters of our inversions, and we employ the conventional scaling relationship for other parameters to shear wave velocity (e.g., Panning & Romanowicz, 2006) based on the earlier work by Montagner & Anderson (1989). Radial anisotropy parameter ξ for shear wave is then computed as $\xi = (\beta_H/\beta_V)^2$

In our inverse problem, we suppose that the observed data $\mathbf{d}$ can be expressed as a function of model parameters $\mathbf{p}$ as, $\mathbf{d} = \mathbf{g}(\mathbf{p})$. The model parameter vector at the $(k+1)$th iteration can then be given as follows (Tarantola & Valette, 1982),

$$\mathbf{p}_{k+1} = \mathbf{p}_0 + \mathbf{C}_{pp}\mathbf{G}_k^T \left(\mathbf{C}_{dd} + \mathbf{G}_k\mathbf{C}_{pp}\mathbf{G}_k^T\right)^{-1} \left[\mathbf{d} - \mathbf{g}\left(\mathbf{p}_k\right) + \mathbf{G}_k\left(\mathbf{p}_k - \mathbf{p}_0\right)\right], \tag{4.1}$$

where $\mathbf{p}_k$ is the model vector at the k-th iteration, $\mathbf{p}_0$ is a reference model vector, $\mathbf{C}_{dd}$ is the *a priori* data covariance matrix, and $\mathbf{C}_{pp}$ is the *a priori* model covariance matrix. $\mathbf{G}_k$ is the kernel matrix that consists of the partial derivatives of the data with respect to the model parameters. For the i-th data and j-th model parameter, the kernel matrix component can be represented as, $G_{ij} = \partial d_i/\partial p_j$. In this study, the elements of the kernel matrix are the partial derivatives (or vertical sensitivity kernels) of phase speeds with respect to anisotropic S-wave speeds, including the scaled sensitivity kernels for other parameters, including P-wave speeds and density.

The *a priori* model covariance matrix, C_{pp}, can be represented by a Gaussian distribution as follows,

$$C_{pp}\left(r_i, r_j\right) = \sigma_m\left(r_i\right)\sigma_m\left(r_j\right)\exp\left\{-\frac{1}{2}\frac{\left(r_i - r_j\right)^2}{L^2}\right\}, \tag{4.2}$$

where r_i is the depth of the i-th model parameter, $\sigma_m(r_i)$ is the standard deviation for the i-th model parameter and L is the average correlation length between the model parameters r_i and r_j.

The standard deviation, $\sigma_m(r_i)$ (hereafter, σ_m^i), controls the amplitude of variations in model parameters for each iteration, and the correlation length L constrains the smoothness of model variations in the depth range, which controls how rapidly the model can vary as a function of depth. The values of these parameters are determined empirically with *a priori* knowledge of the Earth structure.

In this study, we employ the homogeneous background Earth model as the reference structure for the inversion. Following the convention used in the inversion for actual Earth, we set the *a priori* parameters to be $\sigma_i = 0.015$ km/s and $L = 5$ km in the crust (down to 35 km depth), and $\sigma_i = 0.025$ km/s with $L = 20$ km between Moho and 120 km depth, where stochastic heterogeneity is added in most cases of this study. Then, we gradually reduce σ_i and increase L for deeper structure, as $\sigma_i = 0.02$ km/s and $L = 20$ km at 150 – 200 km depth, $\sigma_i = 0.015$ km/s, and $L = 30$ km at 200 – 300 km depth. The maximum depth for the model parameter is set to 400 km since our 2-D models vertically extend down to the 360 km depth only. The parameters at the bottom layer of 300 – 400 km depth are set to $\sigma_i = 0.01$ km/s and $L = 40$ km.

4.1.2 Surface-wave dispersion data for inversions

As discussed in Chapter 3, the absolute values of phase speeds derived from the single-station measurements using the waveforms from the 2-D FDM simulations are affected by the intrinsic limitations of the 2-D FDM approach, especially for long-period Rayleigh waves. However, such numerical effects are expected to commonly affect all the 2-D simulations for both homoge-

neous and heterogeneous models. Thus, by simply taking the difference of measured phase speeds between the heterogeneous and homogeneous models, such numerical effects can be canceled out, and the resultant phase speed perturbations should keep only the influence from the stochastic random heterogeneity.

In this chapter, we employ the phase speed perturbations of the Rayleigh and Love waves measured for the 2-D heterogeneous models with respect to the 2-D homogeneous model, explained in Chapter 3.2.1 for varying strength of heterogeneity. These perturbations are added to the reference phase speeds for the 1-D spherical earth model calculated using MINEOS (Masters et al., 2011) and used as synthetic dispersion data of the inversions for radially anisotropic S-wave models.

4.1.3 Results of inversions

Figs. 4.1 - 4.4 displays the results of inversions for SV and SH velocities (β_V and β_H), and the corresponding radial anisotropy parameter $\xi = (\beta_H/\beta_V)^2$, using the phase speed perturbations in Chapter 3.2.1 for the four models with different strength of heterogeneities. The results of dispersion curve fitting are also shown in each figure.

In these inversions, we used the phase speeds of the fundamental-mode Love and Rayleigh waves for the period range from 30 to 100 s. Therefore, the vertical resolution for deeper structures is limited since the fundamental-mode Love waves in this period range have limited sensitivity to structures below 100 km depth (Fig. 1.1). Note that Rayleigh waves have sufficient sensitivities to the deeper structures below 150 km, but as discussed in Chapter 3.2, our Rayleigh wave measurements in the longer period are somewhat affected by the intrinsic limitations of our 2-D FDM modeling, since we considered the depth range above 360 km in our 2-D models. Therefore, in the

subsequent discussion, we will focus on the shallower structure above 100 km depth, for which our dispersion data sets have sufficient resolving power to estimate the radial anisotropy. To discuss the average radial anisotropy in a certain heterogeneous model, we compute the average value of radial anisotropy ξ in the depth range from 35 to 100 km, which will be discussed in the next section.

The results of inversions show that, in the depth range of the heterogeneous layer (35 – 120 km), the retrieved SV-wave velocity is slower than the reference S-wave velocity, while the SH wave generally remains the same as the reference. The strength of radial anisotropy for the case $\sigma = 0.1$ ($\sigma_{eff} \approx 0.13$) in Fig. 4.1 is the largest with the average value of $\xi \sim 1.07$ in the depth range of 35 – 100 km, which corresponds to about 3.5 % velocity differences between SH and SV wave velocities. For the smaller values of σ, the radial anisotropy becomes significantly weaker; for example, for $\sigma = 0.05$ ($\sigma_{eff} \approx 0.066$) case in Fig. 4.2, the average ξ in the depth range of 35 – 100 km is about 1.02, which is equivalent to about 1 % differences between SH and SV velocities. The model with $\sigma = 0.02$ ($\sigma_{eff} \approx 0.026$) in Fig. 4.3 and $\sigma = 0.01$ ($\sigma_{eff} \approx 0.013$) in Fig. 4.4 shows much weaker radial anisotropy of about 1.007 and 1.003, respectively.

Among all these retrieved models, the peak value for radial anisotropy ξ appears at around 60 km depth, which is in the mid-depth range of the stochastic heterogeneity layer of our 2-D simulations used in Chapter 3.3. These results reflect the character of phase speed perturbations in Fig. 3.14 that indicates the largest perturbation at around 40 s period, for which the fundamental-mode Rayleigh wave has a peak sensitivity at around the 60 km depth.

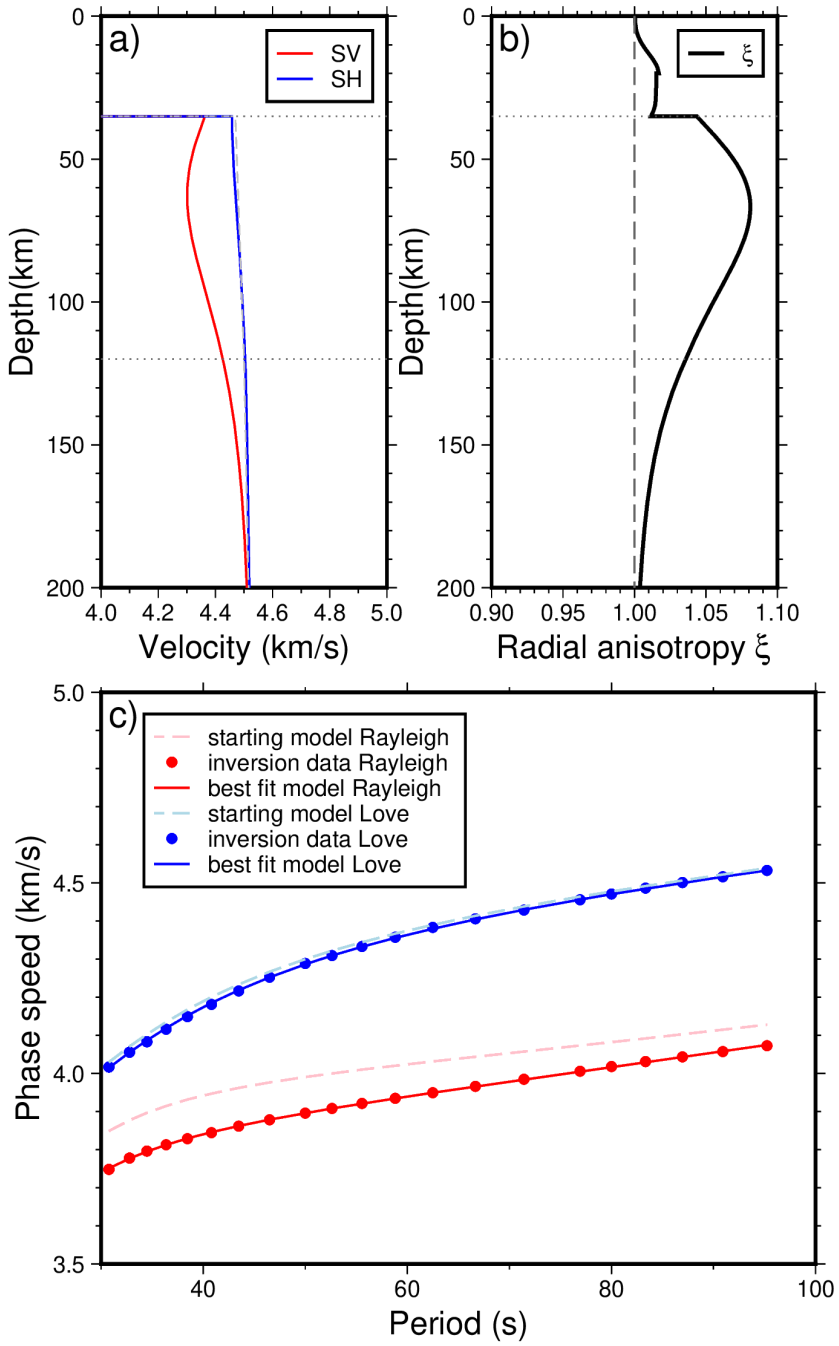

Figure 4.1: Inversion result using the average phase speed perturbations of Rayleigh and Love waves for the heterogeneous model with $a_x = 5$ km, $a_z = 0.5$ km, $\sigma = 0.1$ ($\sigma_{eff} = 0.13$) in Chap. 3.3.1. (a) Retrieved SV (red) and SH (blue) velocities. A dashed grey line shows the isotropic reference S-wave model. (b) Radial anisotropy parameter $\xi = (\beta_H/\beta_V)^2$. A dashed line shows the isotropic case with $\xi = 1$. The depth range of laminated heterogeneities is 35 – 120 km, shown with horizontal dotted lines. Average radial anisotropy in the 35 – 100 km depth range is $\xi = 1.0698$. (c) Results of dispersion curve fitting for the fundamental-mode Rayleigh and Love waves.

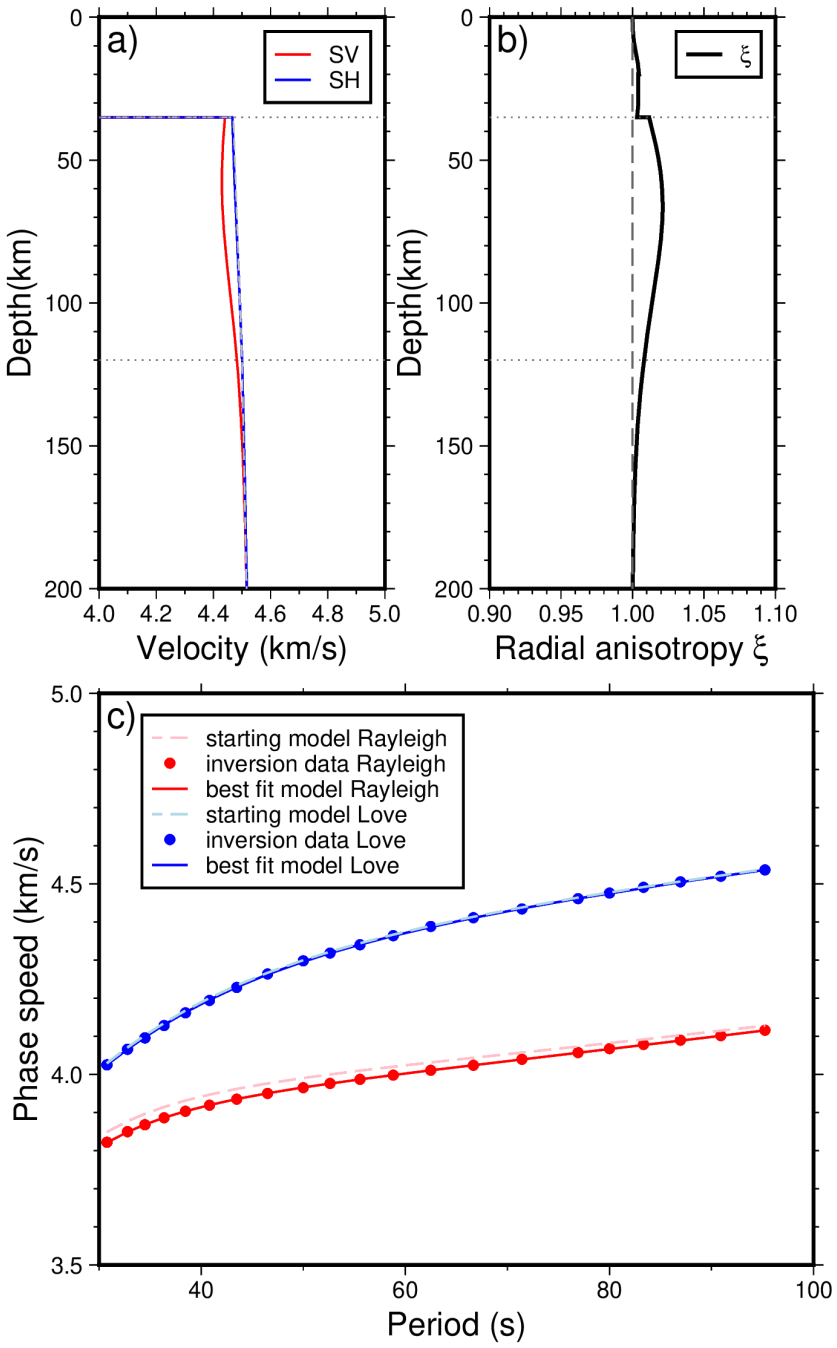

Figure 4.2: Same as Fig. 4.1, but for the heterogeneous model with $\sigma = 0.05$ ($\sigma_{eff} = 0.0659$). Average radial anisotropy in the 35 – 100 km depth range is $\xi = 1.0181$.

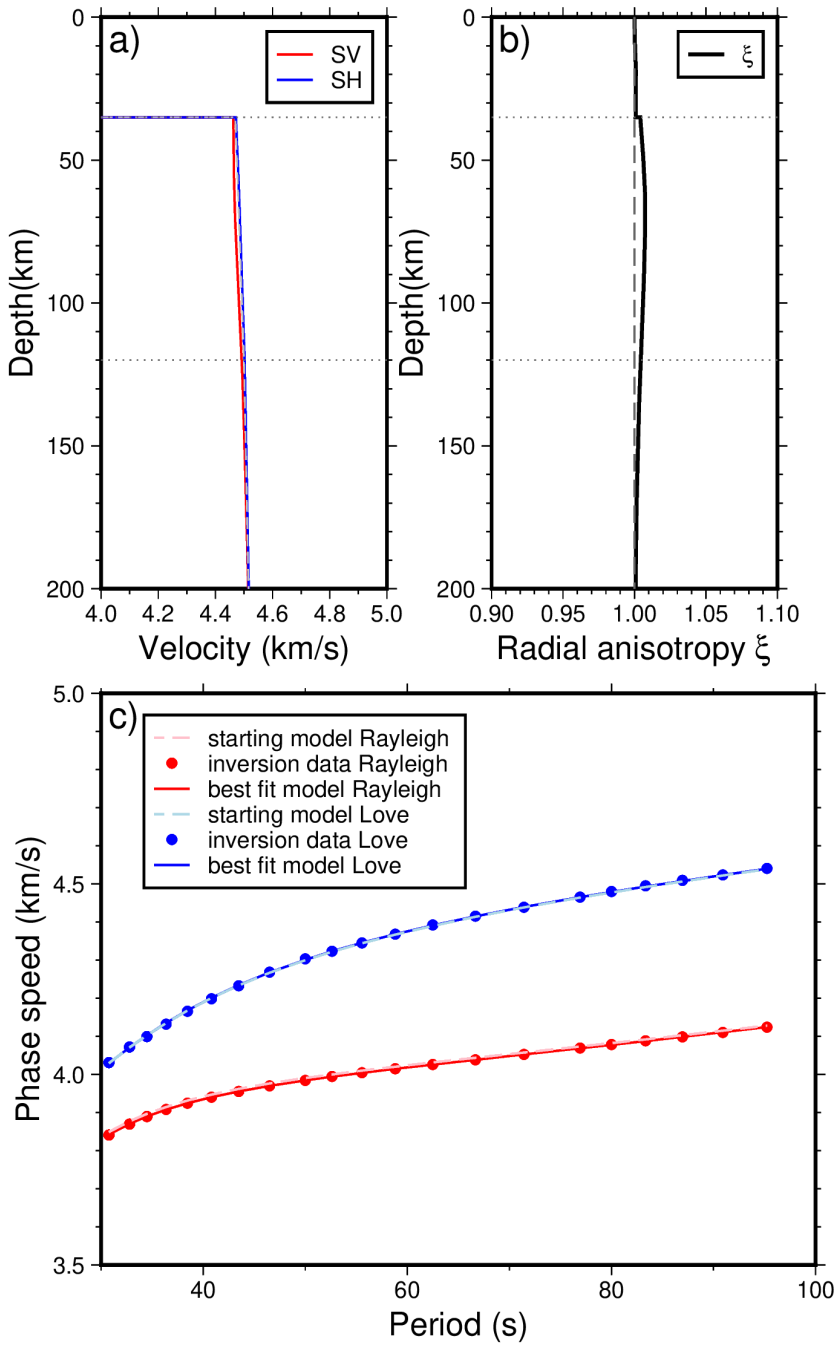

Figure 4.3: Same as Fig. 4.1, but for the heterogeneous model with $\sigma = 0.02$ ($\sigma_{eff} = 0.0263$). Average radial anisotropy in the 35 – 100 km depth range is $\xi = 1.0066$.

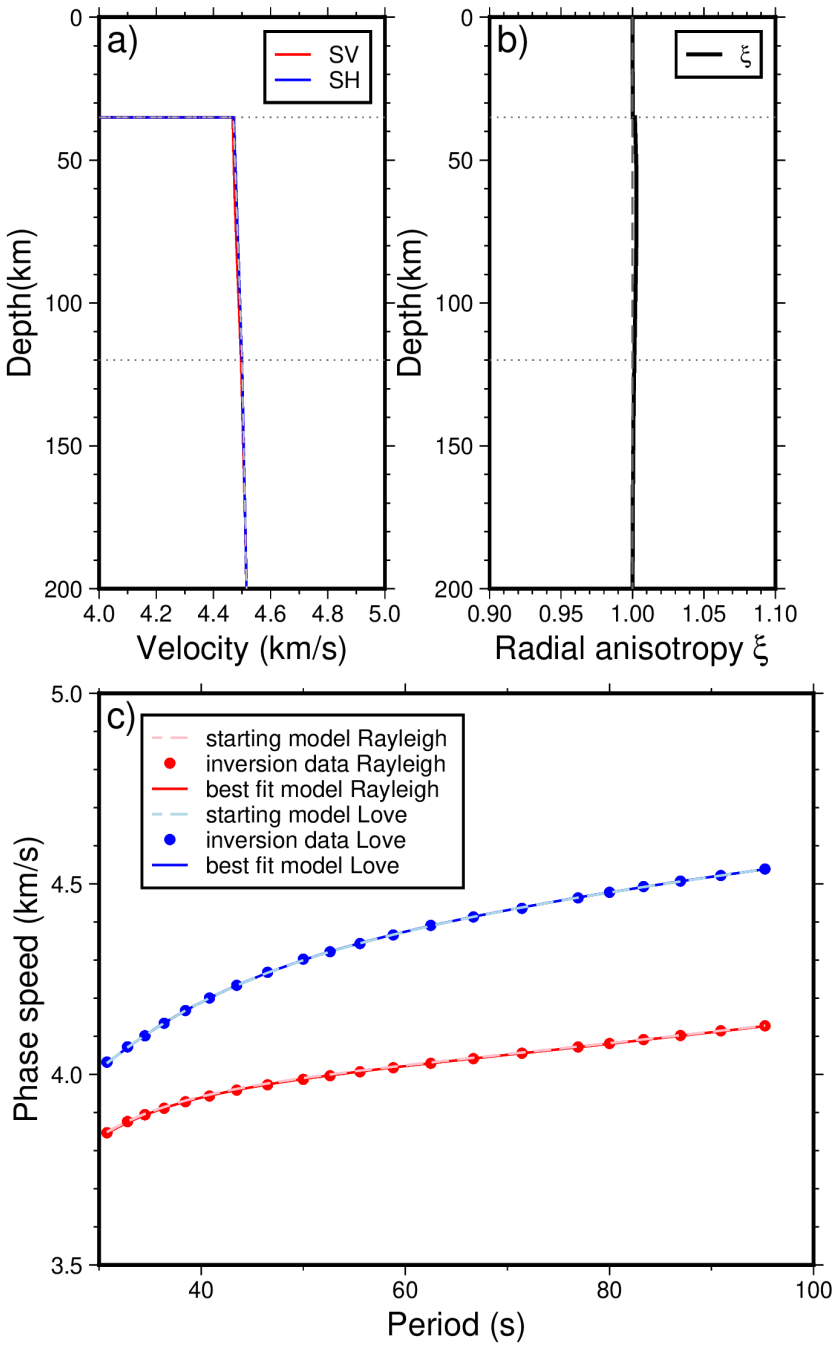

Figure 4.4: Same as Fig.4.3, but for the heterogeneous model with $\sigma = 0.01$ ($\sigma_{eff} = 0.0131$). Average radial anisotropy in the 35 – 100 km depth range is $\xi = 1.0025$.

4.2 Radial anisotropy induced by laminated stochastic heterogeneity

The relationship between the effective velocity fluctuation σ_{eff} and radial anisotropy ξ derived from our inversions in the previous section is summarized in Fig. 4.5. The best-fit curve with the third-degree polynomial is also displayed. Although our data set is limited to only 4 cases of different σ_{eff}, this summary diagram indicates how much of the apparent radial anisotropy ξ can be caused by the effective velocity fluctuations σ_{eff} in 2-D heterogeneous media. Apparently, radial anisotropy ξ increases rapidly as σ_{eff} becomes large.

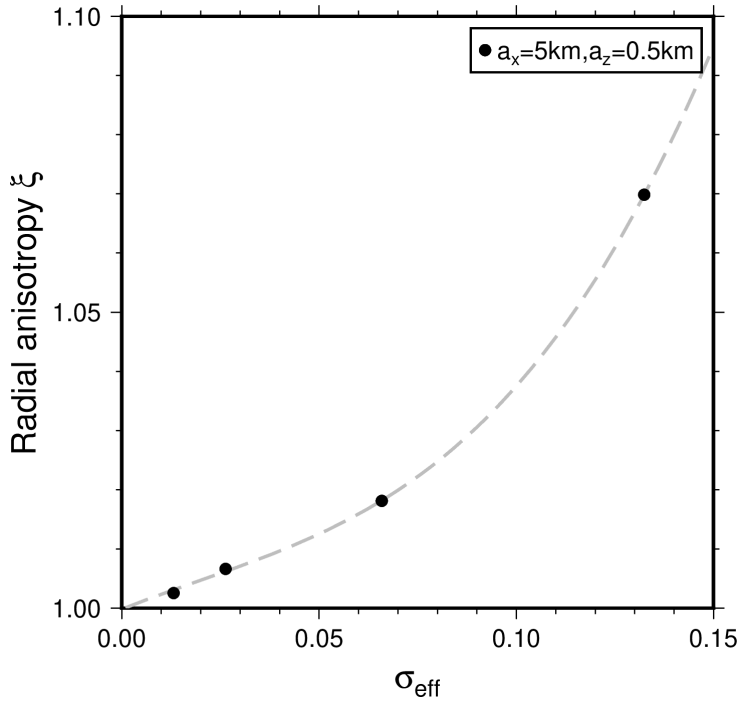

Figure 4.5: Relationship between the effective velocity fluctuations σ_{eff} and resultant radial anisotropy ξ. We incorporated inversion results for four heterogeneous models shown in Figs. 4.1 - 4.4 with $a_x = 5$ km and $a_z = 0.5$ km. Black dots represent the average radial anisotropy ξ in the depth range from 35 to 100 km of the inverted radial anisotropy model. A dashed line is a best-fit curve with the third-degree polynomial.

In this chapter, we have considered the selected cases for varying σ_{eff} with fixed a_x (= 5 km) and a_z (= 0.5 km). However, as shown in Fig. 3.20, the changes in horizontal correlation length a_x also have some influence on phase speed perturbations, although such effects can be relatively weaker compared with the varying σ_{eff} case. Such an effect of changing horizontal scales may partly contribute to the generation of apparent radial anisotropy from finely laminated heterogeneity.

As we reviewed in Chapter 1, some earlier seismological studies suggested the existence of about 1–2 % velocity fluctuations for the quasi-laminar heterogeneity in the lithosphere (e.g., Nielsen et al., 2003; Kennett, 2015; Kennett et al., 2017). From our results summarized in Fig. 3.16 and Fig. 4.5, such weak velocity fluctuations of 1–2 % would cause only a minor effect on surface-wave phase speeds, and the resultant apparent radial anisotropy is almost negligible (0.3–0.7 %).

On the other hand, some theoretical studies expected somewhat greater apparent radial anisotropy of about 3 % (e.g., Fichtner et al., 2013; Kennett & Furumura, 2016) in the lithospheric mantle. From our estimation in Fig. 4.5, in order to create 3 % apparent radial anisotropy, we may need approximately 8 % of velocity fluctuations of laminated heterogeneity, which seems somewhat unlikely over a greater scale but may be possible locally. Note that a greater correlation length of a_x would require somewhat milder velocity fluctuations to generate a similar level of radial anisotropy, as discussed above.

There are some other causes of apparent anisotropy, such as aligned cracks (Thomsen, 1995; Hudson et al., 2001) and/or partial melts (Kawakatsu et al., 2009; Hirschmann, 2010). They can cause relatively larger velocity fluctuations, especially under the existence of melts or fluids. If they exist over wide areas, like melt layers under the oceanic lithosphere (Kawakatsu et al., 2009),

they may generate non-negligible influence on surface-wave dispersion and may induce a certain amount of apparent radial anisotropy in the asthenosphere as observed beneath the Pacific ocean (e.g., Nettles & Dziewoński, 2008; Isse et al., 2019).

Although it is not straightforward to separate the influence from the intrinsic and apparent (or extrinsic) anisotropy in observed radial anisotropy, our numerical approach may be of help in understanding such an issue. Observed radial anisotropy in the upper mantle tomography can reach about 8 %, which is commonly seen in recent tomographic models (e.g., Yoshizawa, 2014; Isse et al., 2019). Our result in Fig. 4.5 indicates that half of such observed radial anisotropy (i.e., about 4 %) may arise from the fine-scale laminated heterogeneities when such stochastic heterogeneities with $\sigma_{eff} = 0.1$ exist in certain areas in the Earth. The effect of laminated random heterogeneity on apparent radial anisotropy can be quantitatively estimated through our numerical approach to waveform modeling, incorporating stochastic heterogeneity. This may not be discussed based solely on the effective medium theory (such as the Backus average in Chapter 2.1) since it tends to have limitations in treating the influence of strong random heterogeneity on surface-wave dispersion (e.g, Capdeville & Marigo, 2007; Dalton et al., 2019).

Chapter 5

Conclusions and future directions

5.1 Summary of the thesis

In this study, we performed a series of 1-D and 2-D numerical experiments to investigate the influence of layered or laminated stochastic heterogeneity on surface-wave phase speeds, which can be a partial cause of the observed radial anisotropy on a large scale. The results from 1-D layered models have suggested that the fluctuations in isotropic shear velocity profiles indeed generate the Rayleigh wave phase speed reduction while Love waves are nearly unaffected, which leads to the apparent radial anisotropy.

Using the 2-D FDM simulations of seismic wavefields in laminated heterogeneous models, we measured the surface-wave phase speeds using the single-station method (Yoshizawa & Kennett, 2002; Yoshizawa & Ekström, 2010). We calculated the ensemble average of reliable single-station measurements from all virtual stations in the epicentral distance range of 900 – 1900 km. Although there are some intrinsic limitations in the 2-D FDM waveform modeling, such as the limited model space, numerical dispersion, and boundary reflections, these numerical effects can be common in both homogeneous and heterogeneous 2-D models. By taking the difference between average phase speeds for the homogeneous and heterogeneous models, such numerical effects can be canceled out. Hence we can extract the aver-

age phase speed perturbations in the period range from 30 to 100 s, caused purely by the laminated random heterogeneity.

Multiple models with heterogeneity with different stochastic parameters were used to quantify the effects on the Rayleigh wave phase speeds. By fixing all the other parameters and allowing only one parameter to change at a time, we found that both the strength (i.e., the standard deviation σ of velocity fluctuation) and shape (the horizontal correlation length a_x) of heterogeneity could have a non-negligible influence on the average velocity perturbation of the fundamental-mode Rayleigh waves. Changing the thickness of the heterogeneous layer causes minor variations of phase speed perturbations, simply reflecting the period-dependent vertical sensitivities of surface waves. For heterogeneous models with fixed σ, we could extract the relationship between the phase speed perturbations and the effective velocity fluctuations σ_{eff} of the 2-D models, suggesting that the Rayleigh wave phase speed tends to decrease rapidly as σ_{eff} becomes greater.

The measured phase speed perturbations (30–100 s) in heterogeneous media were then used to invert for the radially anisotropic 1-D S-velocity profiles. The retrieved vertical profiles of radial anisotropy ξ showed a peak anomaly at around 60 km depth, near the middle depth of the heterogeneous layer (35 – 120 km). Using the average ξ value derived from the retrieved 1-D profiles, we could finally derive a diagram between ξ and σ_{eff} for the stochastic heterogeneity model with $a_x = 5$ km and $a_z = 0.5$ km. This diagram suggests that 5 % velocity fluctuations would cause positive radial anisotropy of over 1 %.

In this study, we have considered the influence of fine-scale heterogeneity with stochastic velocity fluctuations and how they can affect the surface-wave phase speeds and apparent (or structure-induced) radial anisotropy. These stochastic models may not perfectly represent the actual structure

of the Earth. Nevertheless, we could obtain potentially useful information about the effects of horizontally elongated stochastic heterogeneity on long-period surface waves, which can be the basis for interpreting observed seismic anisotropy from surface wave tomography.

5.2 Future directions

To further improve the current study, we summarize several topics to be tackled in the future.

5.2.1 Incorporating realistic 3-D waveform modeling

Incorporating the realistic Earth model and actual events would allow us to directly compare our simulation results with observed data, which may be useful for further discussion. As discussed in Chapter 3.2.3, the results from 2-D FDM simulation contain some numerical effects, which could be improved by constructing a full 3-D spherical Earth model to avoid such influences of limited model space in 2-D, boundary reflections, or Earth flattening approximation. Besides, it is also preferable to perform a 3-D simulation in which the effects of both vertical and horizontal variations can be fully considered.

5.2.2 Model parameters and numerical considerations

We have not carefully considered the effect of density and anelasticicy (Q) due to the lack of sufficient constraints, but they may also have some influence on surface wave dispersion. Moreover, to properly consider the effects of random heterogeneity generated from certain random seeds, the 2-D simulation needs to be repeatedly performed with more different random seeds, although we have employed only 5 models to extract the ensemble average. Incorporating a large number of models with different random seeds would allow us to

achieve a more precise estimation of the ensemble average for a variety of stochastic model parameter sets.

5.2.3 Higher modes and measurement techniques

Although the current measurement technique for surface-wave dispersion has provided us with reliable estimations of the fundamental-mode Rayleigh and Love wave phase speeds, it could be more helpful if we could retrieve multi-mode phase speeds. In particular, the higher-mode information can be of help in improving the inversions for radial anisotropy over a wide depth range (e.g., Yoshizawa, 2014; Taira & Yoshizawa, 2020).

Also, in this study, we used the single-station measurements, which reflect the path-averaged phase speeds between the source and receiver. However, it may also be useful to incorporate multiple types of phase speed measurements, such as the inter-station methods (e.g., Hamada & Yoshizawa, 2015) and the array analysis (e.g., Matsuzawa & Yoshizawa, 2019), which can provide more localized information within the model.

5.2.4 Multi-scale heterogeneity

Kennett & Furumura (2016) have suggested that the real Earth structure should include both fine-scale (<10 km) and medium-scale (10 – 100 km) heterogeneities, which may cause significant radial anisotropy in the lower frequency while creating the waveguide effects required for the extended coda observed. We have also performed numerical simulations for seismic wavefields with such multi-scale heterogeneity (see Appendix A). However, considering the correlation length of medium-scale heterogeneity, it tends to cause biased models (i.e., generating large-scale deterministic structural variations rather than fine-scale stochastic heterogeneity), which would largely affect surface wave propagation. Therefore, the current approach for wave-

form modeling with limited numbers of random seed models, in combination with the waveform analysis for dispersion measurements, may not be sufficient to deal with the medium-scale heterogeneity properly. Thus, more extensive numerical experiments incorporating many different types of random models will be required for further investigation.

Appendix A

Effects of the multi-scale heterogeneity

The actual heterogeneity in the Earth can be represented by significantly varying stochastic parameters both vertically and horizontally, and its existence is unlikely to be limited inside the lithosphere. P wave reflectivity studies (Kennett, 2015) have suggested the existence of strong heterogeneity (about 4 % deviation) with longer horizontal correlation length (>20 km) near the LAT (Lithosphere-Asthenosphere Transition) by Yoshizawa (2014). Kennett et al. (2017) used a multi-scale model with both fine-scale and medium-scale heterogeneities to simulate seismic wave propagation of high-frequency signals and suggested that such multi-scale heterogeneity may contribute to the wide range of structural features such as apparent discontinuity and effective radial anisotropy.

Here we employ similar parameters to Kennett et al. (2017) for constructing models with multi-scale heterogeneities, allowing them to vary in a reasonable range. We combined fine-scale heterogeneity (a_{x1} = 5 km, a_{z1} = 0.5 km, $\sigma_1 = 0.02$) in the depth range from 35 km to 120 km), and medium-scale heterogeneity (a_{x2} = 100 km, a_{z2} = 24 km, σ_2 varies from 0.005 to 0.02) in the depth range from 0 km to 300 km (Table A.1). Here we only allow the strength of medium-scale heterogeneity (σ_2) to vary, so we can directly investigate the effects of medium-scale heterogeneity. Note that, in this appendix, we omit the considerations of the effective strength of velocity

fluctuations (σ_{eff}) for simplicity. We used different random seeds for generating medium-scale and fine-scale heterogeneities. However, the results of phase speed measurements shown here are not the ensemble average of 5 models with different random seeds (like the results in Chapter 3) but from a single model.

The resultant phase speed perturbations are shown in Figs. A.1. The results show that medium-scale heterogeneity significantly influences Rayleigh wave dispersion. For the case with σ_2=0.005, it generates a maximum phase speed drop of about 0.6 %, while the earlier model with fine-scale heterogeneity (σ_1=0.02) only exhibits less than 0.2 % difference (see, Fig. 3.14). For the model with σ_2=0.01, the phase speed perturbation becomes almost double with the maximum phase speed drop of about 1.2 %. When we use the same level of medium and fine-scale heterogeneities (σ_2=0.02), the phase speed perturbation becomes over 2 %, which is close to the case only with unrealistically strong fine-scale heterogeneity ($\sigma = 0.1$).

These experiments suggest that the medium-scale heterogeneity in the model with multi-scale heterogeneity may have much stronger effects on Rayleigh-wave dispersion curves compared with a similar level of fine-scale heterogeneity. Introducing such multi-scale stochastic heterogeneity to the background velocity structure would generate a non-negligible phase speed drop (over 2 %) for the fundamental-mode Rayleigh wave, even with a reasonable size of velocity fluctuations.

However, considering the correlation length used for medium-scale heterogeneity (a_{x2} = 100 km, a_{z2} = 24 km), it may no longer be considered as a "fine scale". This means that the phase speed perturbations of the fundamental mode Rayleigh waves may not simply be arisen from the laminated structure but simply from the large-scale random fluctuation in the model (e.g., slow velocity anomaly in the shallower part and fast velocity anomaly

in the deeper part in the average or effective heterogeneity model). Therefore, the current result may be insufficient to conclude that the medium-scale heterogeneity would have more influence on the apparent radial anisotropy. Additional numerical experiments with many different random models would be required to fully take account of such effects of multi-scale heterogeneities.

	Depth range	a_x	a_z	σ_1
Model 1	35 – 120 km	5 km	0.5 km	0.02
Model 2	35 – 120 km	5 km	0.5 km	0.02
Model 3	35 – 120 km	5 km	0.5 km	0.02
	Depth range	a_x	a_z	σ_2
Model 1	0 – 300 km	100 km	24 km	0.005
Model 2	0 – 300 km	100 km	24 km	0.01
Model 3	0 – 300 km	100 km	24 km	0.02

Table A.1: Model parameters for multi-scale stochastic heterogeneity including both fine (top) and medium (bottom) scale parameters used in Fig. A.1 – A.2. Only σ_2 is allowed to vary, and other parameters are fixed.

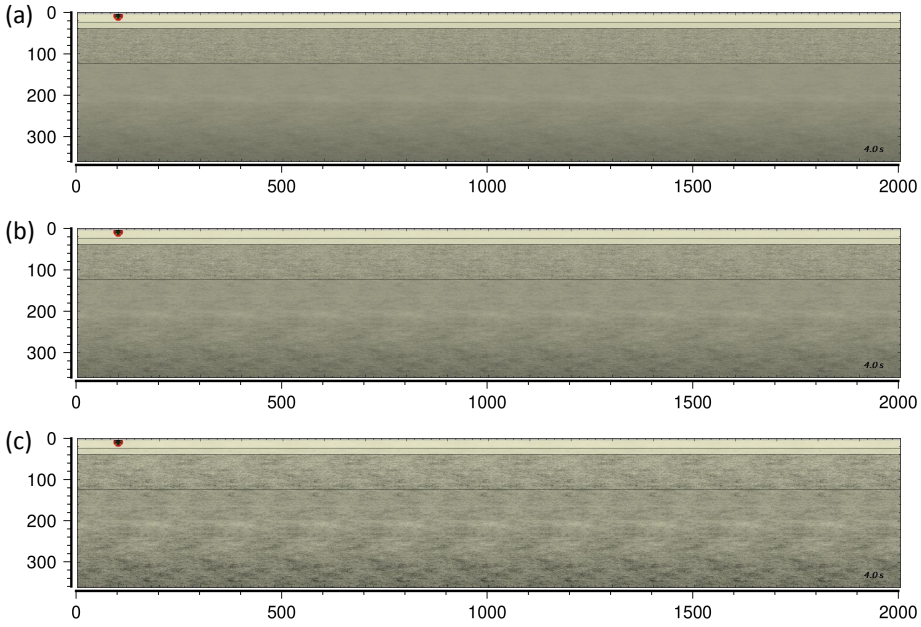

Figure A.1: 2-D heterogeneous models with multi-scale stochastic heterogeneity. We used both fine-scale heterogeneity ($a_{x1} = 5$ km, $a_{z1} = 0.5$ km, $\sigma_1 = 0.02$, depth range from 35 km to 120 km) and medium-scale heterogeneity ($a_{x2} = 100$ km, $a_{z2} = 24$ km, σ_2 varies from 0.005 to 0.02, depth range from 0 km to 300 km).

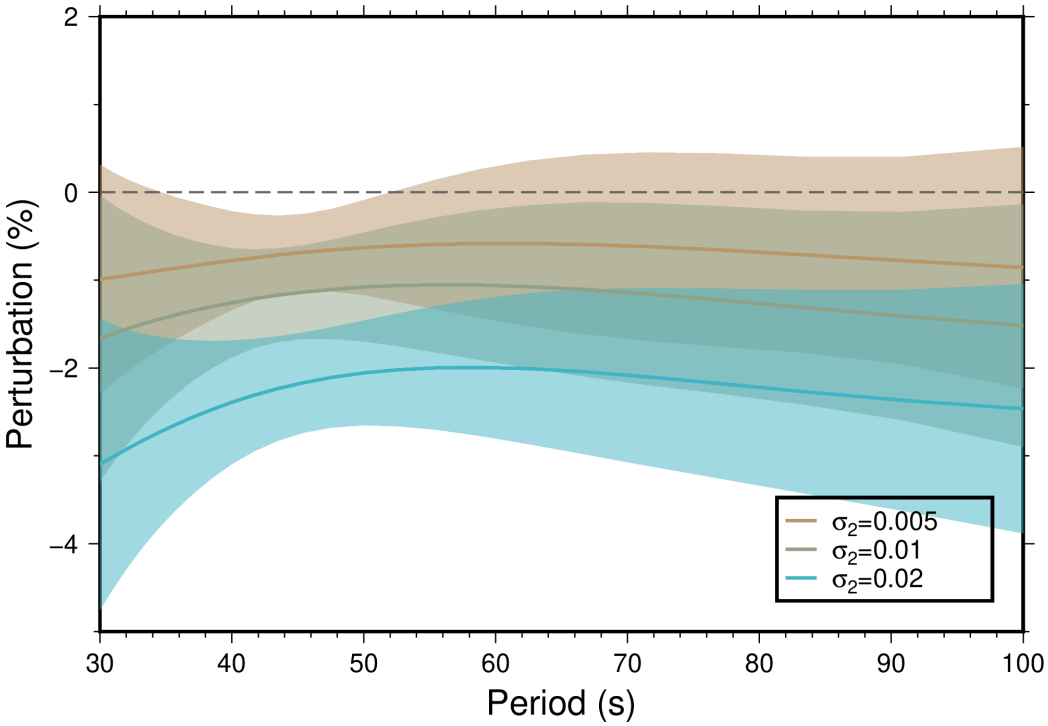

Figure A.2: Same as Fig. 3.14 (average phase speed perturbations for the Rayleigh wave relative to the homogeneous case), but for the multi-scale heterogeneous model in Fig. A.1.

Bibliography

Aki, K., 1968. Seismological evidences for the existence of soft thin layers in the upper mantle under Japan, *Journal of Geophysical Research*, **73**(2), 585–594.

Allegre, C. J. & Turcotte, D. L., 1986. Implications of a two-component marble-cake mantle, *Nature*, **323**, 123–127.

Babuska, V. & Cara, M., 1991. *Seismic Anisotropy in the Earth*, Springer Netherlands, Dordrecht.

Backus, G. E., 1962. Long-wave elastic anisotropy produced by horizontal layering, *Journal of Geophysical Research*, **67**(11), 4427–4440.

Birkey, A., Ford, H. A., Dabney, P., & Goldhagen, G., 2021. The lithospheric architecture of australia from seismic receiver functions, *Journal of Geophysical Research: Solid Earth*, **126**(4), e2020JB020999.

Bodin, T., Capdeville, Y., Romanowicz, B., & Montagner, J. P., 2015. Interpreting radial anisotropy in global and regional tomographic models, *The Earth's Heterogeneous Mantle: A Geophysical, Geodynamical, and Geochemical Perspective*, pp. 105–144.

Capdeville, Y. & Marigo, J.-J., 2007. Second order homogenization of the elastic wave equation for non-periodic layered media, *Geophysical Journal International*, **170**(2), 823–838.

Capdeville, Y., Stutzmann, É., Wang, N., & Montagner, J. P., 2013. Residual homogenization for seismic forward and inverse problems in layered media, *Geophysical Journal International*, **194**(1), 470–487.

Cerjan, C., Kosloff, D., Kosloff, R., & Reshef, M., 1985. A nonreflecting boundary condition for discrete acoustic and elastic wave equations, *GEOPHYSICS*, **50**(4), 705–708.

Dalton, D. R., Meehan, T. B., & Slawinski, M. A., 2019. On backus average in modelling guided waves, *Journal of Applied Geophysics*, **170**, 103815.

Dziewonski, A. M. & Anderson, D. L., 1981. Preliminary reference Earth model, *Physics of the Earth and Planetary Interiors*, **25**(4), 297–356.

Ekström, G., 2011. A global model of Love and Rayleigh surface wave dispersion and anisotropy, 25-250s, *Geophysical Journal International*, **187**(3), 1668–1686.

Ekström, G., Tromp, J., & Larson, E. W. F., 1997. Measurements and global models of surface wave propagation, *Journal of Geophysical Research: Solid Earth*, **102**(B4), 8137–8157.

Faccenda, M., Ferreira, A. M. G., Tisato, N., Lithgow-Bertelloni, C., Stixrude, L., & Pennacchioni, G., 2019. Extrinsic Elastic Anisotropy in a Compositionally Heterogeneous Earth's Mantle, *Journal of Geophysical Research: Solid Earth*, **124**(2), 1671–1687.

Fichtner, A., Kennett, B. L. N., & Trampert, J., 2013. Separating intrinsic and apparent anisotropy, *Physics of the Earth and Planetary Interiors*, **219**, 11–20.

Fishwick, S., Heintz, M., Kennett, B. L. N., Reading, A. M., & Yoshizawa, K., 2008. Steps in lithospheric thickness within eastern

australia, evidence from surface wave tomography, *Tectonics*, **27**(4), doi:10.1029/2007TC002116.

Ford, H. A., Fischer, K. M., Abt, D. L., Rychert, C. A., & Elkins-Tanton, L. T., 2010. The lithosphere–asthenosphere boundary and cratonic lithospheric layering beneath australia from sp wave imaging, *Earth and Planetary Science Letters*, **300**(3), 299–310.

Foster, A., Nettles, M., & Ekström, G., 2014. Overtone Interference in Array-Based Love-Wave Phase Measurements, *Bulletin of the Seismological Society of America*, **104**(5), 2266–2277.

Frankel, A. & Clayton, R. W., 1986. Finite difference simulations of seismic scattering: Implications for the propagation of short-period seismic waves in the crust and models of crustal heterogeneity, *Journal of Geophysical Research*, **91**(B6), 6465.

Furumura, T. & Kennett, B. L. N., 2005. Subduction zone guided waves and the heterogeneity structure of the subducted plate: Intensity anomalies in northern Japan, *Journal of Geophysical Research: Solid Earth*, **110**(10), 1–27.

Gung, Y., Panning, M., & Romanowicz, B., 2003. Global anisotropy and the thickness of continents, *Nature*, **422**(6933), 707–711.

Hamada, K. & Yoshizawa, K., 2015. Interstation phase speed and amplitude measurements of surface waves with nonlinear waveform fitting: Application to USArray, *Geophysical Journal International*, **202**(3), 1463–1482.

Hirschmann, M. M., 2010. Partial melt in the oceanic low velocity zone, *Physics of the Earth and Planetary Interiors*, **179**(1-2), 60–71.

Hudson, J. A., Pointer, T., & Liu, E., 2001. Effective-medium theories for fluid-saturated materials with aligned cracks, *Geophysical Prospecting*, **49**(5), 509–522.

Igel, H., 2016. *Computational Seismology: A Practical Introduction*, Oxford University Press, Oxford.

Isse, T., Kawakatsu, H., Yoshizawa, K., Takeo, A., Shiobara, H., Sugioka, H., Ito, A., Suetsugu, D., & Reymond, D., 2019. Surface wave tomography for the pacific ocean incorporating seafloor seismic observations and plate thermal evolution, *Earth and Planetary Science Letters*, **510**, 116–130.

Jordan, T. H., 2015. An effective medium theory for three-dimensional elastic heterogeneities, *Geophysical Journal International*, **203**(2), 1343–1354.

Kawakatsu, H., Kumar, P., Takei, Y., Shinohara, M., Kanazawa, T., Araki, E., & Suyehiro, K., 2009. Seismic evidence for sharp lithosphere-asthenosphere boundaries of oceanic plates, *Science*, **324**(5926), 499–502.

Kennett, B. L. N., 2015. Lithosphere-asthenosphere P-wave reflectivity across Australia, *Earth and Planetary Science Letters*, **431**, 225–235.

Kennett, B. L. N. & Engdahl, E. R., 1991. Traveltimes for global earthquake location and phase identification, *Geophysical Journal International*, **105**(2), 429–465.

Kennett, B. L. N. & Furumura, T., 2008. Stochastic waveguide in the lithosphere: Indonesian subduction zone to Australian craton, *Geophysical Journal International*, **172**(1), 363–382.

Kennett, B. L. N. & Furumura, T., 2013. High-frequency Po/So guided waves in the oceanic lithosphere: I-long-distance propagation, *Geophysical Journal International*, **195**(3), 1862–1877.

Kennett, B. L. N. & Furumura, T., 2015. Toward the reconciliation of seismological and petrological perspectives on oceanic lithosphere heterogeneity, *Geochemistry, Geophysics, Geosystems*, **16**(9), 3129–3141.

Kennett, B. L. N. & Furumura, T., 2016. Multiscale seismic heterogeneity in the continental lithosphere, *Geochemistry, Geophysics, Geosystems*, **17**(3), 791–809.

Kennett, B. L. N., Fichtner, A., Fishwick, S., & Yoshizawa, K., 2013. Australian seismological referencemodel (AuSREM): Mantle component, *Geophysical Journal International*, **192**(2), 871–887.

Kennett, B. L. N., Yoshizawa, K., & Furumura, T., 2017. Interactions of multi-scale heterogeneity in the lithosphere: Australia, *Tectonophysics*, **717**, 193–213.

Magali, J. K., Bodin, T., Hedjazian, N., Ricard, Y., Capdeville, Y., & Debayle, E., 2021. Quantifying Intrinsic and Extrinsic Contributions to Radial Anisotropy in Tomographic Models, *Journal of Geophysical Research: Solid Earth*, **126**(10), 1–26.

Masters, G., Woodhouse, J. H., & Freeman, G., 2011. Mineos v1.0.2 [software manual], *Computational Infrastructure for Geodynamics*, https://geodynamics.org/cig/software/mineos.

Matsuzawa, H. & Yoshizawa, K., 2019. Array-based analysis of multimode surface waves: application to phase speed measurements and modal waveform decomposition, *Geophysical Journal International*, **218**(1), 295–312.

Maupin, V. & Park, J., 2015. 1.09 - theory and observations - seismic anisotropy, in Treatise on Geophysics (Second Edition), pp. 277–305, ed. Schubert, G., Elsevier, Oxford.

Montagner, J. P. & Anderson, D. L., 1989. Petrological constraints on seismic anisotropy, *Physics of the Earth and Planetary Interiors*, **54**(1-2), 82–105.

Nettles, M. & Dziewoński, A. M., 2008. Radially anisotropic shear velocity structure of the upper mantle globally and beneath North America, *Journal of Geophysical Research: Solid Earth*, **113**(2), 1–27.

Nielsen, L., Thybo, H., Levander, A., & Solodilov, L. N., 2003. Origin of upper-mantle seismic scattering - Evidence from Russian peaceful nuclear explosion data, *Geophysical Journal International*, **154**(1), 196–204.

Nishimura, C. E. & Forsyth, D. W., 1989. The anisotropic structure of the upper mantle in the Pacific, *Geophysical Journal International*, **96**(2), 203–229.

Panning, M. & Romanowicz, B., 2006. A three-dimensional radially anisotropic model of shear velocity in the whole mantle, *Geophysical Journal International*, **167**(1), 361–379.

Reuss, A., 1929. Berechnung der Fließgrenze von Mischkristallen auf Grund der Plastizitätsbedingung für Einkristalle ., *ZAMM - Journal of Applied Mathematics and Mechanics / Zeitschrift für Angewandte Mathematik und Mechanik*, **9**(1), 49–58.

Robertsson, J. O., Blanch, J. O., & Symes, W. W., 1994. Viscoelastic finite-difference modeling, *Geophysics*, **59**(9), 1444–1456.

Sambridge, M., 1999. Geophysical inversion with a neighbourhood algorithm—I. Searching a parameter space, *Geophysical Journal International*, **138**(2), 479–494.

Sun, W. & Kennett, B. L. N., 2017. Mid-lithosphere discontinuities beneath

the western and central North China Craton, *Geophysical Research Letters*, **44**(3), 1302–1310.

Sun, W., Fu, L. Y., Saygin, E., & Zhao, L., 2018. Insights Into Layering in the Cratonic Lithosphere Beneath Western Australia, *Journal of Geophysical Research: Solid Earth*, **123**(2), 1405–1418.

Taira, T. & Yoshizawa, K., 2020. Upper-mantle discontinuities beneath Australia from transdimensional Bayesian inversions using multimode surface waves and receiver functions, *Geophysical Journal International*, **223**(3), 2085–2100.

Takeuchi, H. & Saito, M., 1972. Seismic Surface Waves, in Seismology: Surface Waves and Free Oscillations, vol. 11, pp. 217–295, ed. Bolt, B. A., Academic Press, New York.

Tarantola, A. & Valette, B., 1982. Generalized nonlinear inverse problems solved using the least squares criterion, *Reviews of Geophysics and Space Physics*, **20**(2), 219–232.

Thomsen, L., 1995. Elastic anisotropy due to aligned cracks in porous rock, *Geophysical Prospecting*, **43**(6), 805–829.

Voigt, W., 1928. *Lehrbuch der Kristallphysik*, Teubner Verlag, Leipzig.

Wang, N., Montagner, J. P., Fichtner, A., & Capdeville, Y., 2013. Intrinsic versus extrinsic seismic anisotropy: The radial anisotropy in reference Earth models, *Geophysical Research Letters*, **40**(16), 4284–4288.

Yoshizawa, K., 2002. *Development and Application of New Techniques for Surface Wave Tomography*, Ph.D. thesis, Australian National University, pp 204.

Yoshizawa, K., 2014. Radially anisotropic 3-D shear wave structure of the Australian lithosphere and asthenosphere from multi-mode surface waves, *Physics of the Earth and Planetary Interiors*, **235**, 33–48.

Yoshizawa, K. & Ekström, G., 2010. Automated multimode phase speed measurements for high-resolution regional-scale tomography: Application to North America, *Geophysical Journal International*, **183**(3), 1538–1558.

Yoshizawa, K. & Kennett, B. L. N., 2002. Non-linear waveform inversion for surface waves with a neighbourhood algorithm - application to multimode dispersion measurements, *Geophysical Journal International*, **149**, 118–133.

Yoshizawa, K. & Kennett, B. L. N., 2015. The lithosphere-asthenosphere transition and radial anisotropy beneath the Australian continent, *Geophysical Research Letters*, **42**(10), 3839–3846.

Yuan, H. & Romanowicz, B., 2010. Lithospheric layering in the North American craton, *Nature*, **466**(7310), 1063–1068.